Forlenza MJ, Miller GE. Increased serum levels of 8-hydroxy-2'-deoxyguanosine in clinical depression. Psychosom Med 2006;68:1–7.
Fransen E, D'Hooge R, Van Camp G, Verhoye M, Sijbers J, Reyniers E, et al. L1 knockout mice show dilated ventricles, vermis hypoplasia and impaired exploration patterns. Hum Mol Genet 1998;7:999–1009.
Gass P, Reichardt HM, Strekalova T, Henn F, Tronche F. Mice with targeted mutations of glucocorticoid and mineralocorticoid receptors: models for depression and anxiety? Physiol Behav 2001;73:811–25.
Gennarini G, Hirsch MR, He HT, Hirn M, Finne J, Goridis C. Differential expression of mouse neural cell-adhesion molecule (N-CAM) mRNA species during brain development and in neural cell lines. J Neurosci 1986;6:1983–90.
Grant NJ, Claudepierre T, Aunis D, Langley K. Glucocorticoids and nerve growth factor differentially modulate cell adhesion molecule L1 expression in PC12 cells. J Neurochem 1996;66:1400–8.
He HT, Barbet J, Chaix JC, Goridis C. Phosphatidylinositol is involved in the membrane attachment of NCAM-120, the smallest component of the neural cell adhesion molecule. EMBO J 1986;5:2489–94.
Hemperly JJ, DeGuglielmo JK, Reid RA. Characterization of cDNA clones defining variant forms of human neural cell adhesion molecule N-CAM. J Mol Neurosci 1990;2:71–8.
Hemperly JJ, Edelman GM, Cunningham BA. cDNA clones of the neural cell adhesion molecule (N-CAM) lacking a membrane-spanning region consistent with evidence for membrane attachment via a phosphatidylinositol intermediate. Proc Natl Acad Sci U S A 1986;83:9822–6.
Heuser IJ, Schweiger U, Gotthardt U, Schmider J, Lammers CH, Dettling M, et al. Pituitary-adrenal-system regulation and psychopathology during amitriptyline treatment in elderly depressed patients and normal comparison subjects. Am J Psychiatry 1996;153:93–9.
Holsboer F. The corticosteroid receptor hypothesis of depression. Neuropsychopharmacology 2000;23:477–501.
Ivanova SA, Semke VY, Vetlugina TP, Rakitina NM, Kudyakova TA, Simutkin GG. Signs of apoptosis of immunocompetent cells in patients with depression. Neurosci Behav Physiol 2007;37:527–30.
Kallunki P, Edelman GM, Jones FS. Tissue-specific expression of the L1 cell adhesion molecule is modulated by the neural restrictive silencer element. J Cell Biol 1997;138:1343–54.
Kiss JZ, Muller D. Contribution of the neural cell adhesion molecule to neuronal and synaptic plasticity. Rev Neurosci 2001;12:297–310.
Knable MB, Barci BM, Webster MJ, Meador-Woodruff J, Torrey EF. Molecular abnormalities of the hippocampus in severe psychiatric illness: postmortem findings from the Stanley Neuropathology Consortium. Mol Psychiatry 2004;9(544):609–20.
Laifenfeld D, Karry R, Grauer E, Klein E, Ben-Shachar D. Antidepressants and prolonged stress in rats modulate CAM-L1, laminin, and pCREB, implicated in neuronal plasticity. Neurobiol Dis 2005a;20:432–41.
Laifenfeld D, Karry R, Klein E, Ben-Shachar D. Alterations in cell adhesion molecule L1 and functionally related genes in major depression: a postmortem study. Biol Psychiatry 2005b;57:716–25.
Lampen A, Grimaldi PA, Nau H. Modulation of peroxisome proliferator-activated receptor delta activity affects neural cell adhesion molecule and polysialyltransferase ST8SiaIV induction by teratogenic valproic acid analogs in F9 cell differentiation. Mol Pharmacol 2005;68:193–203.
Law JW, Lee AY, Sun M, Nikonenko AG, Chung SK, Dityatev A, et al. Decreased anxiety, altered place learning, and increased CA1 basal excitatory synaptic transmission in mice with conditional ablation of the neural cell adhesion molecule L1. J Neurosci 2003;23:10419–32.
Martin KC, Kandel ER. Cell adhesion molecules, CREB, and the formation of new synaptic connections. Neuron 1996;17:567–70.
Matsubara T, Funato H, Kobayashi A, Nobumoto M, Watanabe Y. Reduced glucocorticoid receptor alpha expression in mood disorder patients and first-degree relatives. Biol Psychiatry 2006;59:689–95.
McEwen BS. Stress and hippocampal plasticity. Annu Rev Neurosci 1999;22:105–22.
Murray BA, Owens GC, Prediger EA, Crossin KL, Cunningham BA, Edelman GM. Cell surface modulation of the neural cell adhesion molecule resulting from alternative mRNA splicing in a tissue-specific developmental sequence. J Cell Biol 1986;103:1431–9.
Nelson MD, Saykin AJ, Flashman LA, Riordan HJ. Hippocampal volume reduction in schizophrenia as assessed by magnetic resonance imaging: a meta-analytic study. Arch Gen Psychiatry 1998;55:433–40.
Ongur D, Drevets WC, Price JL. Glial reduction in the subgenual prefrontal cortex in mood disorders. Proc Natl Acad Sci U S A 1998;95:13290–5.
Paratcha G, Ledda F, Ibanez CF. The neural cell adhesion molecule NCAM is an alternative signaling receptor for GDNF family ligands. Cell 2003;113:867–79.
Pariante CM, Miller AH. Glucocorticoid receptors in major depression: relevance to pathophysiology and treatment. Biol Psychiatry 2001;49:391–404.
Perlman WR, Webster MJ, Kleinman JE, Weickert CS. Reduced glucocorticoid and estrogen receptor alpha messenger ribonucleic acid levels in the amygdala of patients with major mental illness. Biol Psychiatry 2004;56:844–52.
Pike JL, Irwin MR. Dissociation of inflammatory markers and natural killer cell activity in major depressive disorder. Brain Behav Immun 2006;20:169–74.
Plenge P, Mellerup ET, Jorgensen OS. Lithium treatment regimens induce different changes in [3H]paroxetine binding protein and other rat brain proteins. Psychopharmacology (Berl) 1992;106:131–5.
Poltorak M, Frye MA, Wright R, Hemperly JJ, George MS, Pazzaglia PJ, et al. Increased neural cell adhesion molecule in the CSF of patients with mood disorder. J Neurochem 1996;66:1532–8.
Ricard CS, Pena JD, Hernandez MR. Differential expression of neural cell adhesion molecule isoforms in normal and glaucomatous human optic nerve heads. Brain Res Mol Brain Res 1999;74:69–82.
Roubin R, Deagostini-Bazin H, Hirsch MR, Goridis C. Modulation of NCAM expression by transforming growth factor-beta, serum, and autocrine factors. J Cell Biol 1990;111:673–84.
Sadoul K, Meyer A, Low MG, Schachner M. Release of the 120 kDa component of the mouse neural cell adhesion molecule N-CAM from cell surfaces by phosphatidylinositol-specific phospholipase C. Neurosci Lett 1986;72:341–6.
Sandi C. Stress, cognitive impairment and cell adhesion molecules. Nat Rev Neurosci 2004;5:917–30.
Sandi C, Merino JJ, Cordero MI, Touyarot K, Venero C. Effects of chronic stress on contextual fear conditioning and the hippocampal expression of the neural cell adhesion molecule, its polysialylation, and L1. Neuroscience 2001;102:329–39.
Sandi C, Bisaz R. A model for the involvement of neural cell adhesion molecules in stress-related mood disorders. Neuroendocrinology 2007;85:158–76.
Sapolsky RM. Glucocorticoids and hippocampal atrophy in neuropsychiatric disorders. Arch Gen Psychiatry 2000;57:925–35.
Schachner M. Neural recognition molecules and synaptic plasticity. Curr Opin Cell Biol 1997;9:627–34.
Schoenherr CJ, Anderson DJ. The neuron-restrictive silencer factor (NRSF): a coordinate repressor of multiple neuron-specific genes. Science 1995;267:1360–3.
Schoenherr CJ, Paquette AJ, Anderson DJ. Identification of potential target genes for the neuron-restrictive silencer factor. Proc Natl Acad Sci U S A 1996;93:9881–6.
Seidel A, Arolt V, Hunstiger M, Rink L, Behnisch A, Kirchner H. Increased CD56+ natural killer cells and related cytokines in major depression. Clin Immunol Immunopathol 1996;78:83–5.
Sheline YI, Sanghavi M, Mintun MA, Gado MH. Depression duration but not age predicts hippocampal volume loss in medically healthy women with recurrent major depression. J Neurosci 1999;19:5034–43.
Simpson CS, Morris BJ. Regulation of neuronal cell adhesion molecule expression by NF-kappa B. J Biol Chem 2000;275:16879–84.
Soares JC, Mann JJ. The anatomy of mood disorders—review of structural neuroimaging studies. Biol Psychiatry 1997;41:86–106.
Stork O, Welzl H, Cremer H, Schachner M. Increased intermale aggression and neuroendocrine response in mice deficient for the neural cell adhesion molecule (NCAM). Eur J Neurosci 1997;9:1117–25.
Stork O, Welzl H, Wotjak CT, Hoyer D, Delling M, Cremer H, et al. Anxiety and increased 5-HT1A receptor response in NCAM null mutant mice. J Neurobiol 1999;40:343–55.
Takebayashi M, Hisaoka K, Nishida A, Tsuchioka M, Miyoshi I, Kozuru T, et al. Decreased levels of whole blood glial cell line-derived neurotrophic factor (GDNF) in remitted patients with mood disorders. Int J Neuropsychopharmacol 2006;9:607–12.
Thomas AJ, Davis S, Ferrier IN, Kalaria RN, O'Brien JT. Elevation of cell adhesion molecule immunoreactivity in the anterior cingulate cortex in bipolar disorder. Biol Psychiatry 2004;55:652–5.
Thomas AJ, Ferrier IN, Kalaria RN, Davis S, O'Brien JT. Cell adhesion molecule expression in the dorsolateral prefrontal cortex and anterior cingulate cortex in major depression in the elderly. Br J Psychiatry 2002;181:129–34.
Tomasiewicz H, Ono K, Yee D, Thompson C, Goridis C, Rutishauser U, et al. Genetic deletion of a neural cell adhesion molecule variant (N-CAM-180) produces distinct defects in the central nervous system. Neuron 1993;11:1163–74.
Torrey EF, Barci BM, Webster MJ, Bartko JJ, Meador-Woodruff JH, Knable MB. Neurochemical markers for schizophrenia, bipolar disorder, and major depression in postmortem brains. Biol Psychiatry 2005;57:252–60.
Touyarot K, Sandi C. Chronic restraint stress induces an isoform-specific regulation on the neural cell adhesion molecule in the hippocampus. Neural Plast 2002;9:147–59.
Vawter MP. Dysregulation of the neural cell adhesion molecule and neuropsychiatric disorders. Eur J Pharmacol 2000;405:385–95.
Vawter MP, Freed WJ, Kleinman JE. Neuropathology of bipolar disorder. Biol Psychiatry 2000;48:486–504.
Vawter MP, Hemperly JJ, Hyde TM, Bachus SE, VanderPutten DM, Howard AL, et al. VASE-containing N-CAM isoforms are increased in the hippocampus in bipolar disorder but not schizophrenia. Exp Neurol 1998;154:1–11.
Vawter MP, Howard AL, Hyde TM, Kleinman JE, Freed WJ. Alterations of hippocampal secreted N-CAM in bipolar disorder and synaptophysin in schizophrenia. Mol Psychiatry 1999;4:467–75.
Venero C, Tilling T, Hermans-Borgmeyer I, Schmidt R, Schachner M, Sandi C. Chronic stress induces opposite changes in the mRNA expression of the cell adhesion molecules NCAM and L1. Neuroscience 2002;115:1211–9.
Watanabe Y, Gould E, McEwen BS. Stress induces atrophy of apical dendrites of hippocampal CA3 pyramidal neurons. Brain Res 1992;588:341–5.
Webster MJ, Knable MB, O'Grady J, Orthmann J, Weickert CS. Regional specificity of brain glucocorticoid receptor mRNA alterations in subjects with schizophrenia and mood disorders. Mol Psychiatry 2002;7(924):985–94.
Webster MJ, Vawter MP, Freed WJ. Immunohistochemical localization of the cell adhesion molecules Thy-1 and L1 in the human prefrontal cortex patients with schizophrenia, bipolar disorder, and depression. Mol Psychiatry 1999;4:46–52.
Wright IC, Rabe-Hesketh S, Woodruff PW, David AS, Murray RM, Bullmore ET. Meta-analysis of regional brain volumes in schizophrenia. Am J Psychiatry 2000;157:16–25.

JCS ePress online publication date 27 January 2009

Drebrin A regulates dendritic spine plasticity and synaptic function in mature cultured hippocampal neurons

Anton Ivanov[1], Monique Esclapez[2], Christophe Pellegrino[1], Tomoaki Shirao[3] and Lotfi Ferhat[1,4,*]

[1]INMED/INSERM U29, Parc Scientifique de Luminy, 13273, Marseille, France
[2]INSERM U 751, Université d'Aix-Marseille, Hôpital de la Timone, Marseille, France
[3]Department of Neurobiology and Behavior, Gunma University Graduate School of Medicine, Maebashi, Gunma, Japan
[4]CNRS UMR 6184, Neurobiologie des Interactions Cellulaires et Neurophysiopathologie (NICN), IFR Jean Roche, Marseille, F-13020, France
*Author for correspondence (e-mail: lotfi.ferhat@univmed.fr)

Accepted 30 October 2008
Journal of Cell Science 122, 524-534 Published by The Company of Biologists 2009
doi:10.1242/jcs.033464

Summary

Drebrin A, one of the most abundant neuron-specific F-actin-binding proteins, is found exclusively in dendrites and is particularly concentrated in dendritic spines receiving excitatory inputs. We investigated the role of drebrin A in synaptic transmission and found that overexpression of drebrin A augmented the glutamatergic synaptic transmission, probably through an increase of active synaptic site density. Interestingly, overexpression of drebrin A also affected the frequency, amplitude and kinetics of miniature inhibitory postsynaptic currents (mIPSCs), despite the fact that GABAergic synapse density and transmission efficacy were not modified. Downregulation of drebrin A led to a decrease of both glutamatergic and GABAergic synaptic activity. In heterologous cells, drebrin A reorganized and stabilized F-actin and these effects were mediated by its actin-binding domain. Thus, drebrin A might regulate dendritic spine morphology via regulation of actin cytoskeleton remodeling and dynamics. Our data demonstrate for the first time that drebrin A modulates glutamatergic and GABAergic synaptic activities.

Supplementary material available online at
http://jcs.biologists.org/cgi/content/full/122/4/524/DC1

Key words: Spine morphogenesis, F-actin, GABA, Glutamate, vGlut1, Gad-65, Bassoon

Introduction

Dendritic spines are the postsynaptic elements that receive the majority of excitatory glutamatergic inputs in the CNS (Harris and Kater, 1994). These small protrusions emerging from dendritic shafts are believed to constitute sites for the development of glutamatergic neuronal networks and might be a cellular substrate for synaptic plasticity (Yuste and Bonhoeffer, 2001).

The actin filament (F-actin) is one of the major structural elements of dendritic spines (Fifkova and Delay, 1982; Matus et al., 1982). These actin filaments are thought to be the key target of molecular mechanisms regulating spine plasticity that has been shown to be activity dependent (Matus, 2000). The adult isoform of drebrin, drebrin A (DA), a major neuron-specific F-actin-binding protein, emerges as a candidate protein that regulates the actin cytoskeleton of dendritic spines (Sekino et al., 2007). DA is specifically localized at dendritic spines of mature cortical neurons (Hayashi et al., 1996; Aoki et al., 2005) and is known to inhibit the actin-binding activity of tropomyosin, fascin and α-actinin (Ishikawa et al., 1994; Sasaki et al., 1996). In vitro, it also inhibits the interaction between actin and myosin (Hayashi et al., 1996; Ishikawa et al., 2007), suggesting that it modulates actin filament contractility. Transfection of DA into fibroblasts induced reorganization of actin filaments, leading to a change in cell morphology (Shirao et al., 1994). Such transfection in neurons results in the elongation of dendritic spines of cortical neurons (Hayashi and Shirao, 1999). Furthermore, downregulation of DA expression in developing hippocampal neurons suppresses the accumulation of F-actin within dendritic spines (Takahashi et al., 2003).

In addition to its role in spine morphology, DA might be involved in spine functions. It has been recently shown that DA is involved in spinous clustering of the postsynaptic density (PSD) scaffold protein, PSD-95 (Takahashi et al., 2003), as well as in the activity-dependent synaptic targeting of N-methyl-D-aspartate (NMDA) subtype of glutamate receptors (Takahashi et al., 2006). Consistent with this observation, the induction of long-term potentiation (LTP) in the hippocampus is accompanied by the enhanced DA content within dendritic spines (Fukazawa et al., 2003). All these data support the hypothesis that DA expressed in spines can modulate synaptic activity.

To test this hypothesis, we investigated the effects of DA on dendritic spine morphology and its consequences on synaptic activity, in mature cultured hippocampal neurons. Our study led to three main conclusions: (1) the actin-binding domain of DA is responsible for dendritic spine plasticity, presumably via regulation of actin cytoskeleton remodeling and dynamics; (2) enhanced expression of DA increases the density of glutamatergic but not GABAergic synapses and leads to alteration of the normal excitatory-inhibitory balance in favour of excitation; (3) downregulation of DA results in the decrease of both glutamatergic and GABAergic synaptic transmissions without affecting the normal excitatory-inhibitory balance. Thus, the present study provides the first evidence that an actin-binding protein such as DA modulates both glutamatergic and GABAergic synaptic transmission in mature hippocampal neurons.

Results

Postsynaptic localization of endogenous DA in mixed hippocampal cultures

The developmental changes of DA localization in hippocampal neurons have been described in low-density culture from 7 to 21 days in vitro (DIV) (Takahashi et al., 2003). In this study, we re-examined this issue in mixed high-density hippocampal cultures (supplementary material Fig. S1A,B). Our data confirmed the postsynaptic localization of DA in mixed hippocampal neurons at 21 DIV, because it colocalized with two specific markers for the postsynaptic compartment, PSD-95 and F-actin, in most spines (supplementary material Fig. S1C-E).

The actin-binding domain of DA is responsible for spine morphological changes induced by overexpression of DA-GFP in mature hippocampal neurons

It has been shown that DA affects some morphological aspects of cortical dendritic spines (Hayashi and Shirao, 1999). To analyze the physiological consequences of morphological changes induced by DA, we re-examined the effects of DA on spine morphology in our mature and high-density hippocampal culture system. As revealed by cotransfected red fluorescent protein (RFP) neurons (Fig. 1A,B), both green fluorescent protein (GFP, used as a control) (Fig. 1A′) and DA-GFP (Fig. 1B′) were distributed within dendritic shafts, as well as in dendritic protrusions. With respect to DA-GFP, the green fluorescence in dendritic shafts was lighter than in dendritic protrusions. Striking morphological changes were observed between dendritic protrusions of DA-GFP- (Fig. 1B′) and those of GFP neurons (Fig. 1A′). Indeed, the dendrites of DA-GFP neurons displayed longer protrusions (Fig. 1B-B″, arrows) compared with those found in GFP neurons (Fig. 1A-A″). Some of these long protrusions reached over 5 μm (see asterisks in Fig. 1B-B″). All protrusions induced by DA-GFP included heads, and thus differed in their morphology from dendritic filopodia, which have no heads. These observations suggested that these long protrusions were spines and were more mature than filopodia, which are precursors of dendritic spines (Papa et al., 1995).

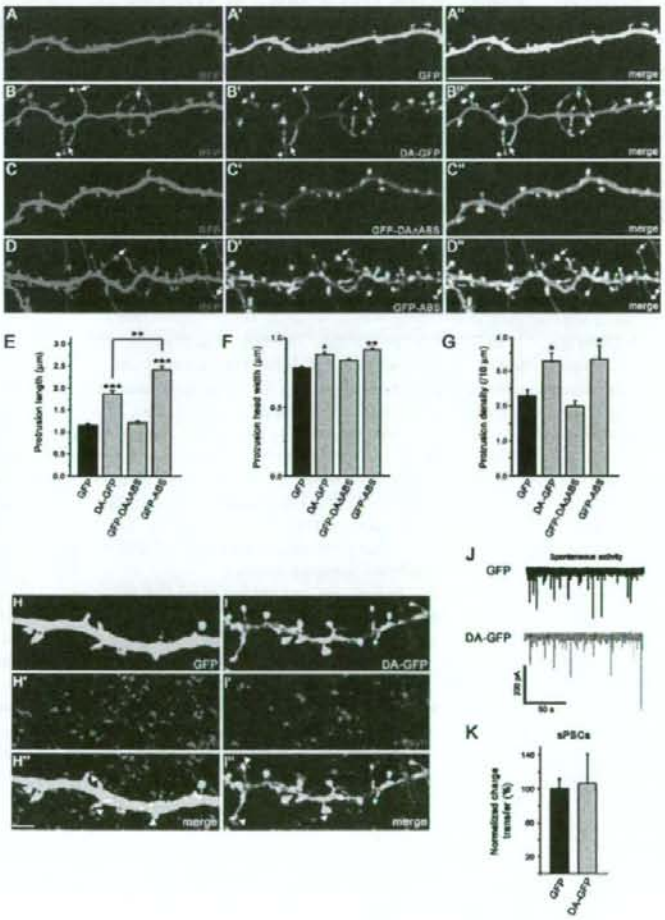

Fig. 1. Effects of DA-GFP overexpression on spine morphology and network activity. Cultured neurons were cotransfected on DIV 21 with RFP (A) and GFP (A′), RFP (B) and DA-GFP (B′), RFP (C) and GFP-DAΔABS (C′), or RFP (D) and GFP-ABS (D′). At 23 DIV, neurons were fixed and then analyzed. RFP channel is shown in all panels to outline dendritic morphology. (A″,B″,C″ and D″) Merged images. Scale bar: 10 μm. (E-G) Quantification of DA-GFP effects on protrusion plasticity. Histograms showing the average length (E), width (F) and density (G) of protrusions of GFP, DA-GFP, GFP-DAΔABS and GFP-ABS neurons. As with GFP spines (H-H″), the long spines induced by DA-GFP (I-I″) were associated with functional excitatory synaptic contacts. GFP (H) or DA-GFP (I) neurons immunostained for synaptophysin (H′ and I′). (H″ and I″) Merged images. Some synaptophysin clusters are not in close apposition to the spines of GFP or DA-GFP neurons because they are probably opposed to dendritic shafts or spines of nontransfected neurons. Scale bar: 10 μm. *P<0.05, **P<0.01, ***P<0.001, Bonferroni's test. (J) Examples of sPSCs recorded at −60 mV in GFP (black trace) and DA-GFP neurons (gray trace). (K) Histogram showing the sPSCs charge transfer in all recorded GFP and DA-GFP neurons. All data in E-G and K are mean ± s.e.m.

To investigate whether DA-GFP exerts its effects via its interaction with F-actin, we cotransfected mature hippocampal neurons with RFP (Fig. 1C) and GFP-DAΔABS (Fig. 1C′), a mutant of DA that lacks the actin-binding domain (Hayashi et al., 1999). As revealed by coexpressed RFP (Fig. 1C), GFP-DAΔABS (Fig. 1C′) was detected in dendritic shafts as well as at dendritic protrusions (Fig. 1C″). In contrast to DA-GFP, GFP-DAΔABS did not induce elongation of dendritic protrusions (Fig. 1C-C″). These data indicate that the elongation of dendritic protrusions induced by DA-GFP requires its actin-binding domain.

We further determined whether the overexpression of the actin-binding domain of DA was sufficient to induce the elongation of dendritic protrusions. For this purpose, we cotransfected hippocampal neurons with RFP (Fig. 1D) and GFP-ABS (Fig. 1D′), a construct that contains only the actin-binding domain of DA (Hayashi et al., 1999). As visualized by cotransfected RFP (Fig. 1D), GFP-ABS was found in dendritic shafts as well as in dendritic protrusions (Fig. 1D″). Similarly to DA-GFP, GFP-ABS induced morphological changes in dendritic protrusions. Indeed, some dendritic protrusions of GFP-ABS neurons were markedly longer (Fig. 1D-D″, see arrows) than those observed in GFP neurons (Fig. 1A-A″). In addition, GFP-ABS neurons displayed long protrusions with heads, reminiscent of dendritic spines. Therefore, the actin-binding domain of DA is necessary and sufficient to induce an effect on dendritic spine elongation.

Quantitative analysis in both DA-GFP and GFP-ABS neurons showed that the average protrusion lengths were significantly longer (1.86±0.08 and 2.40±0.10 μm, respectively) than that in GFP (1.15±0.04 μm; n=10; P<0.001; Bonferroni's test) (Fig. 1E) and GFP-DAΔABS neurons (1.15±0.04 and 1.21±0.04 μm, respectively; n=10; P<0.001; Bonferroni's test) (Fig. 1E). However, the average protrusion length of GFP-DAΔABS neurons was not significantly different from that of GFP neurons (P=0.38; Bonferroni's test) (Fig. 1E). Interestingly, the average protrusion of GFP-ABS was significantly longer than that in DA-GFP neurons (P<0.01; Bonferroni's test) (Fig. 1E), presumably due to their differences in expression levels. Indeed, western blot analyses on CHO-K1 cells showed higher expression levels of GFP-ABS compared with those of DA-GFP construct (data not shown).

In DA-GFP and GFP-ABS neurons, the average protrusion head width was significantly larger (0.88±0.02 and 0.91±0.01 μm, respectively) than that in GFP neurons (0.78±0.02 μm; n=10; P<0.05 for DA-GFP and P<0.01 for GFP-ABS; Bonferroni's test) (Fig. 1F). However, in GFP-DAΔABS neurons, the average protrusion head width (0.83±0.01 μm) was not different from that of GFP neurons (n=10; P=0.18; Bonferroni's test) (Fig. 1F).

In DA-GFP and GFP-ABS neurons, the average protrusion densities were significantly higher (3.28±0.23 and 3.32±0.39 spines/10 μm, respectively) than that in GFP neurons (2.29±0.17 spines/10 μm; n=10; P<0.05; Bonferroni's test) (Fig. 1G), whereas the average protrusion density of GFP-DAΔABS neurons (2.00±0.15 spines/10 μm) was not significantly different from that of GFP neurons (n=10; P=0.26; Bonferroni's test) (Fig. 1G). Therefore the actin-binding domain of DA was necessary and sufficient to induce an effect on spine morphology.

The molecular mechanisms by which DA-GFP causes elongation of dendritic spines was investigated. For this purpose, we overexpressed either DA-GFP or its DA mutants (GFP-DAΔABS and GFP-ABS) in CHO-K1 cells and analyzed its effects on the organization and stabilization of F-actin (supplementary material Figs S2 and S3, respectively). CHO-K1 cells were used because, in contrast to neurons, they provide a model of choice for visualizing the cellular organization and stability of F-actin (Rami et al., 2006). Studies in heterologous cells revealed that DA reorganized F-actin and stabilized them and these effects were dependent upon its actin-binding domain (supplementary material Figs S2 and S3, respectively).

Effects of DA-GFP overexpression on synaptic function

Our confocal microscopy data revealed that as for spines labeled with GFP (Fig. 1H-H″, see arrowheads), the long protrusions induced by DA-GFP (Fig. 1I) were associated with axon terminals since a presynaptic marker such as synaptophysin (Fig. 1I′) was facing most of these dendritic protrusions (Fig. 1I″, arrowheads). The close apposition of the presynaptic marker to the long spines induced by overexpression of DA-GFP suggests the presence of synaptic excitatory contacts. We next investigated whether these synapses were functional. Whole-cell recordings of spontaneous and miniature synaptic currents were performed on mature cultured hippocampal neurons overexpressing either GFP (used as a control, supplementary material Fig. S4) or DA-GFP. Our data showed that spontaneous activity was detected both in GFP or DA-GFP neurons (Fig. 1J), indicating that these neurons were alive and integrated in the neuronal network. In addition, the neuronal network activity was not affected by the overexpression of DA-GFP compared with that of GFP neurons. Indeed, the average charge transfer of spontaneous postsynaptic currents (sPSCs) was not significantly different in both culture types (GFP, 100±11%; DA-GFP, 106±35%; n≥5; P=0.8; U-test) (Fig. 1K).

Next, we investigated whether overexpression of DA-GFP was also associated with changes in the electrophysiological properties of excitatory glutamatergic synapses (Fig. 2A). In DA-GFP neurons, the cumulative probability plots of amplitude (Fig. 2B) and frequency (Fig. 2C) of miniature excitatory postsynaptic currents (mEPSCs) were significantly shifted to higher values compared with those of GFP neurons (n=8; P<0.01 for the amplitude and P<0.05 for the frequency; K-S test). The average amplitude and frequency of mEPSCs were increased in DA-GFP neurons (14.0±0.6 pA; 3.7±0.5 Hz) when compared with those of GFP neurons (11.8±0.4 pA, Fig. 2B, inset; 2.9±0.5 Hz, Fig. 2C, inset). However, the average rise times (GFP: 1.28±0.26 mseconds; DA-GFP: 1.16±0.11 mseconds; n=8; P=0.67; Student's t-test) (Fig. 2D) and decay times (GFP, 6.04±0.90 mseconds; DA-GFP, 6.39±0.79 mseconds; n=8; P=0.14; Student's t-test) (Fig. 2E) were comparable. As a result of the amplitude and frequency changes of mEPSCs in DA-GFP neurons, the average charge transfer of mEPSCs was significantly increased in DA-GFP neurons (334±93 vs 100±20%; n=8; P<0.01; U-test) (Fig. 2F).

The GABA miniature inhibitory postsynaptic currents (mIPSCs) were also recorded from the same GFP and DA-GFP neurons (Fig. 3A) used for mEPSC recordings. Surprisingly, the effects of DA-GFP overexpression on GABA transmission were more severe than those on glutamate transmission. In neurons overexpressing DA-GFP, cumulative probability plots of mIPSC amplitude were significantly shifted to lower values compared with those of GFP neurons (n=8; P<0.01; K-S test) (Fig. 3B). The average amplitude of mIPSCs was lower in DA-GFP neurons (24.0±0.9 pA) than in GFP neurons (34.3±1.8 pA) (Fig. 3B, inset). However, the cumulative probability plots of mIPSC frequency in DA-GFP neurons were significantly shifted to higher values compared with those of GFP neurons (n=8; P<0.001; K-S test) (Fig. 3C). The average frequency of mIPSCs was higher in neurons overexpressing

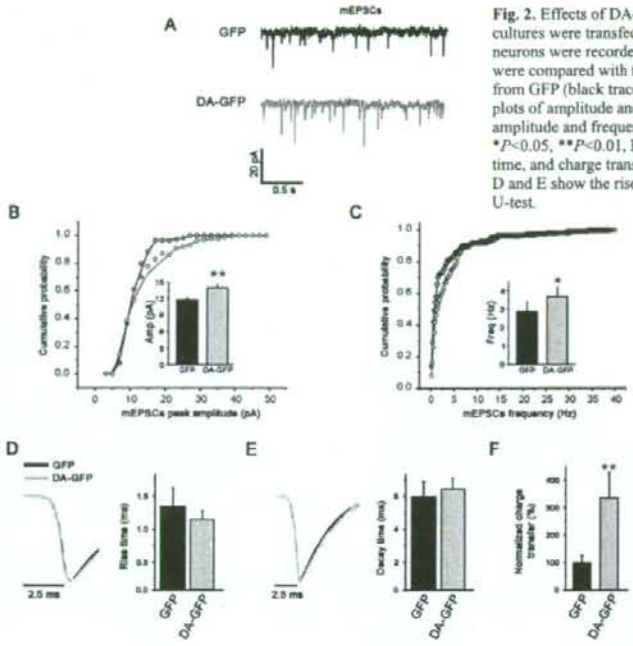

Fig. 2. Effects of DA-GFP overexpression on glutamate function. Mixed hippocampal cultures were transfected at 21 DIV with GFP or DA-GFP, and 1 day later, the transfected neurons were recorded. Electrophysiological recordings of GFP neurons used as controls were compared with those of DA-GFP neurons. (A) Examples of mEPSCs recordings from GFP (black trace) and DA-GFP neurons (gray trace). (B,C) Cumulative probability plots of amplitude and frequency of mEPSCs in GFP and DA-GFP neurons. The average amplitude and frequency of mEPSCs in GFP and DA-GFP neurons are shown as insets. $^{*}P<0.05$, $^{**}P<0.01$, K-S test. (D-F) Histograms showing the average rise time, decay time, and charge transfer of mEPSCs respectively in GFP and DA-GFP neurons. Traces in D and E show the rise and decay time, respectively, of the average mEPSCs. $^{**}P<0.01$, U-test.

DA-GFP (2.8±0.3 Hz) than in GFP neurons (1.3±0.2 Hz; n=8) (Fig. 3C, inset). The average rise time of mIPSCs was significantly increased in DA-GFP neurons (4.28±0.64 mseconds) when compared with that of GFP neurons (1.84±0.16 mseconds; n=8; $P<0.05$; Student's t-test) (Fig. 3D), whereas the average decay time was significantly decreased (18.93±1.46 vs 23.38±2.41 mseconds; n=8; $P<0.05$; Student's t-test) (Fig. 3E). However, despite the mIPSC properties changes described above, the average charge transfer in neurons overexpressing DA-GFP (132±33%) was not significantly different from that of GFP neurons (100±3%; n=8; P=0.23; U-test) (Fig. 3F).

Thus, the overexpression of DA-GFP displayed differential effects on functional properties of excitatory and inhibitory synapses. Indeed, DA enhances the strength of excitatory synaptic transmission preferentially (Fig. 2F), without affecting the efficacy of inhibitory synaptic transmission (Fig. 3F). As a result, the average inhibition to excitation charge transfer ratio was significantly reduced in DA-GFP neurons (5.5±0.2) when compared with that of GFP neurons (11.2±0.5; n=8; $P<0.01$; U-test) (Fig. 3G).

The effects of DA-GFP on synaptic proteins

The changes in GABA and glutamate miniature postsynaptic current (mPSC) properties induced by DA-GFP prompted us to examine whether the density of glutamate and GABA receptors were affected. The quantitative analysis revealed that DA overexpression did not modify significantly the average current density [amplitude (pA)/cell capacitance (pF)] of the agonist-mediated responses compared with that of GFP neurons, which were used as a control (isoguvacine, 8.9±1.8 vs 8.7±2.2, P=0.93; AMPA, 3.9±2.1 vs 6.3±3.7, P=0.39; NMDA, 2.2±0.6 vs 1.8±0.3; $n\geq9$; P=0.37; Student's t-test) (Fig. 4B). These results suggested that the density of GABA$_A$, AMPA, and NMDA membrane receptors were comparable in both GFP and DA-GFP neurons.

We therefore assessed whether postsynaptic expression of DA-GFP might affect the density of glutamatergic and GABAergic presynaptic terminals (Fig. 4C). These terminals were identified with synaptophysin (the general presynaptic marker) or transmitter-specific markers of glutamatergic and GABAergic axons (vGlut1 and Gad-65, respectively). The average densities of synaptophysin and vGlut1 clusters (clusters/10 μm) along dendrites (shafts and/or protrusions) of DA-GFP were not different from those of GFP neurons (syn, 1.1±0.4 vs 1.2±0.4, P=0.7; vGlut1, 3.9±0.4 vs 3.9±0.4, P=0.87; $n\geq32$ dendrites; Student's t-test) (Fig. 4J). However, in DA-GFP neurons, most protrusions (over 98%) were associated with clusters of synaptophysin or vGlut1, suggesting that the majority of protrusions had a presynaptic partner, similar to spines of GFP neurons. Since DA-GFP increased the dendritic spine density and the glutamatergic synaptic activity, we concluded that the density of glutamatergic synapses was increased in DA-GFP neurons.

The postsynaptic expression of DA-GFP did not affect the density of GABA presynaptic terminals in DA-GFP versus GFP neurons (Gad-65, 1.1±0.3 vs 1.2±0.5 clusters/10 μm; $n\geq32$ dendrites; P=0.55; Student's t-test) (Fig. 4J). We next assessed whether the density of GABA synapses was affected in DA-GFP neurons. For this purpose we used β2,3 subunits of the GABA$_A$ receptor as a postsynaptic marker because β2,3 is one of the most abundant subunits of the GABA$_A$ receptors in the brain (McKernan and Whiting, 1996). Our data showed that the average density of clusters (clusters/10 μm) positive for β2,3 or for synaptophysin and β2,3 in DA-GFP was not different from that of GFP neurons (β2,3, 4.8±0.8 vs 4.5±0.8, P=0.51; β2,3 + syn, 1.4±0.5 vs 1.7±0.5, P=0.29; $n\geq32$ dendrites; Student's t-test) (Fig. 4J). Therefore the densities of GABA terminals and synapses were similar in GFP and DA-GFP neurons. Taken together, these data indicated that the ratio of glutamatergic to GABAergic synapses was increased in DA-GFP neurons.

One possible explanation of the absence of significant changes in the density of presynaptic terminals in the presence of such marked changes in the density and shape of postsynaptic spines is that multiple spines can share the same terminal. If this is the case, multiple active zones should form, with a corresponding increase of active zone-associated proteins, such as bassoon. To assess this hypothesis, we studied the effects of DA overexpression on bassoon clusters (Fig. 5A,B$^{\infty}$). Our data showed that the average density of bassoon clusters (clusters/10 μm) along dendrites (shafts and/or protrusions) was increased in DA-GFP (28.2±1.9) compared with that of GFP neurons (16.8±2.0; $n\geq15$ dendrites, $P<0.0001$; Student's

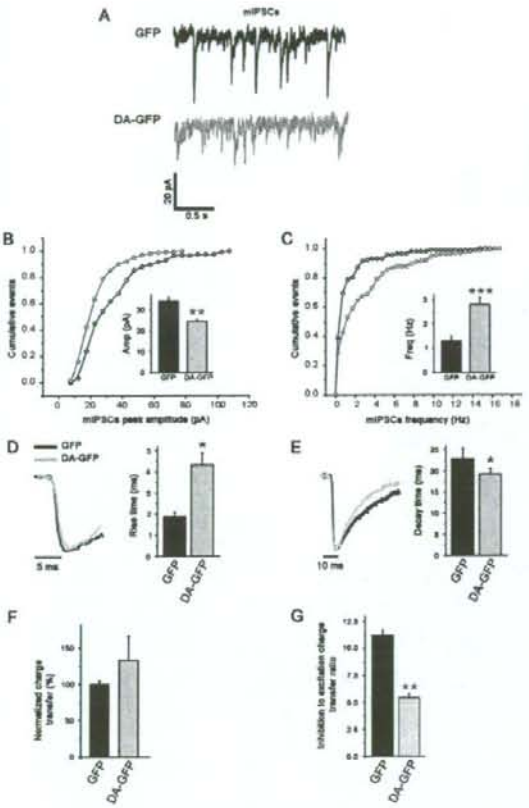

Fig. 3. Effects of DA-GFP overexpression on GABA function. Mixed hippocampal cultures were transfected at 21 DIV with GFP or DA-GFP, and 1 day later, the transfected neurons were recorded. Electrophysiological recordings of GFP neurons used as controls were compared with those of DA-GFP neurons. (A) Examples of mIPSCs recordings from GFP neurons (black trace) and DA-GFP neurons (gray trace). (B,C) Cumulative probability plots of amplitude and frequency of mIPSCs in GFP and DA-GFP neurons. The average amplitude (B) and frequency of mIPSCs (C) in GFP and DA-GFP neurons are shown in insets. $^{**}P<0.01$, $^{***}P<0.001$, K-S test. (D-G) Histograms showing the average rise time, decay time, charge transfer and inhibition to excitation transfer charge ratio of mEPSCs, respectively, in GFP and DA-GFP neurons. $^{*}P<0.05$, *t*-test; $^{**}P<0.01$, U-test.

t-test) (Fig. 5C). Moreover, the average number of bassoon clusters on spines was increased almost twofold in DA-GFP neurons (1.9±0.2 vs 1.0±0.1 clusters/spine; $n \geq 15$ dendrites; $P<0.0001$; Student's *t*-test) (Fig. 5D). From these data, we concluded that indeed the increased number of spines was paralleled by an increase in the number of active zones.

Effects of downregulation of DA expression on synaptic function

Western blot analysis showed that treatment of mature mixed hippocampal cultures with DA antisense oligonucleotides (AS), whose specificity and efficiency have been described previously (Takahashi et al., 2003; Takahashi et al., 2006), reduced significantly the expression of endogenous DA (AS, 11.87±3.47%) when compared with untreated (Ctl, 100.00±14.77%; $n=7$; $P<0.0001$; Bonferroni's test) or sense-treated neurons (S, 84.59±12.91%; $n=7$; $P<0.001$; Bonferroni's test) (Fig. 6A,B, right panel). The expression of another neuronal protein such as β3-tubulin was not altered by oligonucleotide treatments when compared with untreated or sense-treated cultures (Ctl, 100.00±1.15%; S, 100.17±1.84%; AS, 100.21±1.68%; $n=7$; $P=0.99$; ANOVA) (Fig. 6A,B, left panel), in keeping with previously reported data for β-actin (Takahashi et al., 2003; Takahashi et al., 2006).

Whole-cell recordings of spontaneous and miniature synaptic currents were performed on mature cultured hippocampal neurons treated with sense oligonucleotides (used as a control, for details see supplementary material Fig. S4) or antisense oligonucleotides. Both sense and antisense oligonucleotide-treated neurons showed spontaneous activity (Fig. 6C), suggesting that these neurons were alive and fully integrated in the neuronal network. In addition, the neuronal network activity was not affected by the treatment with antisense oligonucleotides compared with that of neurons treated with sense oligonucleotides. Indeed, the average charge transfer of sPSCs was not significantly different in both culture types (S, 100±15%; AS, 92±21%; $n \geq 6$; $P=0.8$; U-test) (Fig. 6D).

The mEPSCs were recorded from S or AS neurons (Fig. 7A). In antisense-treated neurons, the cumulative probability plots of amplitude and frequency of mEPSCs were significantly shifted to lower values when compared to sense-treated neurons ($n=6$; $P<0.05$; K-S test) (Fig. 7B,C). The average amplitude and frequency of mEPSCs were decreased in antisense-treated neurons (11.3±0.9 pA; 4.3±1.5 Hz) when compared with those of sense-treated neurons (12.3±1.0 pA; 6.7±2.1 Hz) (Fig. 7B,C, insets). However, the average rise times (S, 1.44±0.16; AS, 1.58±0.15; $n=6$; $P=0.67$; Student's *t*-test) (Fig. 7D) and decay times (S, 4.42±0.65; AS, 4.67±0.61; $n=6$; $P=0.14$; Student's *t*-test) were comparable (Fig. 7E). As a result of amplitude and frequency changes of mEPSCs in antisense-treated neurons, the average charge transfer of mEPSCs was significantly reduced (56±3 vs 100±15%; $n=6$; $P<0.05$; U-test) (Fig. 7F).

We recorded the GABA mIPSCs from the same oligonucleotide-treated neurons, where the mEPSCs were recorded (Fig. 8A). In antisense-treated neurons, the cumulative probability plots of amplitude and frequency of mIPSCs were significantly shifted to lower values as compared with those of sense-treated neurons ($n=6$; $P<0.01$ for the amplitude and $P<0.05$ for the frequency; K-S test) (Fig. 8B,C). The average amplitude and frequency of mIPSCs were decreased in antisense-treated (15.9±1.6 pA; 2.3±0.7 Hz) when compared to sense-treated neurons (23.2±2.0 pA; 3.1±0.7 Hz) (Fig. 8B,C, insets). The average rise time and decay time of mIPSCs were not significantly modified in antisense-treated (3.52±0.44 mseconds; 20.48±1.78 mseconds) when compared with those of sense-treated neurons (2.74±0.31 mseconds; 22.25±3.30 mseconds; $n=6$; $P=0.12$ and 0.37 respectively; Student's *t*-test) (Fig. 8D,E). Owing to the mIPSC property changes described above, the average charge transfer in antisense-treated neurons was significantly reduced (78±11 vs 100±10%; $n=6$; $P<0.05$; U-test) (Fig. 8F). Thus, the reduction of DA expression affected both the functional properties of glutamatergic and GABAergic synapses. Despite these changes, the inhibition to excitation charge transfer ratio was not altered by the reduction of DA expression (AS, 7.7±2.8; S, 5.1±1.5; $n=6$; $P=0.9$; U-test) (Fig. 8G). Thus, the functional balance between excitation and inhibition was maintained while DA level was reduced.

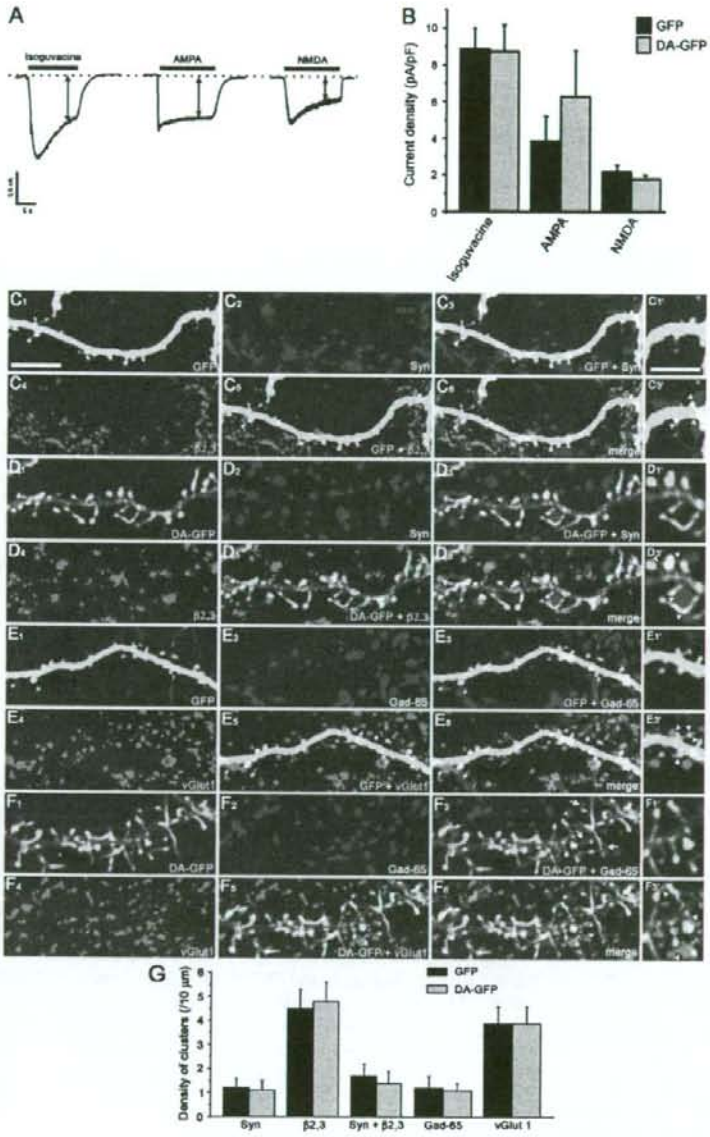

Fig. 4. Effects of DA-GFP on the density of GABA and glutamate receptors and synaptic proteins. Transfected neurons were recorded in whole-cell configuration at –60 mV for $GABA_A$- or AMPA-generated responses and –20 mV for NMDA-mediated current in the presence of TTX and strychnine. (A) Example of current responses induced by bath application of receptor agonists, Isoguvacine (20 µM), AMPA (100 µM) and NMDA (50 µM, with 10 µM glycine, NMDA coactivator) to activate $GABA_A$, AMPA and NMDA receptors, respectively, 10 seconds after starting perfusion (double arrows) with agonist-containing solution. (B) Quantitative analysis revealed that DA overexpression did not modify significantly the average current density of the agonist-mediated responses compared with that of GFP neurons. (C) Mixed hippocampal cultures were transfected at 21 DIV with GFP (C_1,E_1 and insets $C_{1'}$,$E_{1'}$) or DA-GFP (D_1,F_1 and insets $D_{1'}$,$F_{1'}$), and 1 day after transfection, cells were double immunostained for synaptophysin (C_2,D_2) and the subunit β2,3 of $GABA_A$ receptors (C_4,D_4) or for Gad-65 (E_2,F_2) and vGlut1 (E_4,F_4). All the synaptic markers were located either on the dendritic shafts or on dendritic protrusions. Interestingly, we observed in DA neurons that several dendritic spines share the same presynaptic terminal (see arrowheads in $D_{3'}$ vs $C_{3'}$ and $F_{3'}$ vs $E_{3'}$). Scale bars: 10 µm in C_1-F_6 and 5 µm in insets in right column. (G) The average density of syn, β2,3, syn + β2,3, Gad-65 and vGlut1 clusters along dendrites of DA-GFP were not different from those of GFP neurons. Note that in addition to dendrites of transfected neurons, all synaptic markers also stained dendrites of nontransfected neurons.

Discussion

This study provides the first evidence that DA can modulate both glutamatergic and GABAergic synaptic activities through regulation of spine plasticity.

Actin-binding domain of drebrin A is involved in spine plasticity

Our data clearly demonstrate that overexpression of DA increases spine density in mature hippocampal neurons. This finding is in keeping with the work of Takahashi and colleagues (Takahashi et al., 2003; Takahashi et al., 2006), who showed that downregulation of DA by antisense oligonucleotide treatment significantly decreased the density of filopodia spines. Altogether, these data strongly suggest that DA is involved in spine formation. The modification of the dynamic turnover of dendritic spines by stabilisation of F-actin might be one of the possible mechanisms leading to increased spine density. Indeed, we show that DA overexpression in CHO-K1 cells protects F-actin from cytochalasin B destabilization (supplementary material Fig. S3). Consistent with these findings, earlier studies also showed that DA expression in fibroblasts induced cytochalasin-D-resistant actin structures at their adhesion

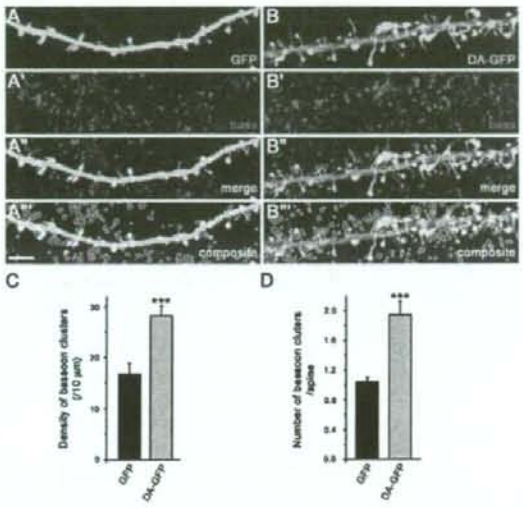

Fig. 5. Effects of DA-GFP overexpression on bassoon protein. Mixed hippocampal cultures were transfected at 21 DIV with GFP (A) or DA-GFP (B) and 1 day after transfection, cells were immunostained for bassoon (A′,B′). (A″ and B″) Merge of panels A and A′ and B and B′, respectively. (A‴ and B‴) Composite of A″ and B″, and drawings showing selected objects obtained with ImageJ software from A′ and B′, respectively. (C,D) Histograms showing the density of bassoon clusters (C) and their number per spine (D) in GFP and DA-GFP neurons. ***P<0.0001, Student's t-test. Scale bar: 5 µm.

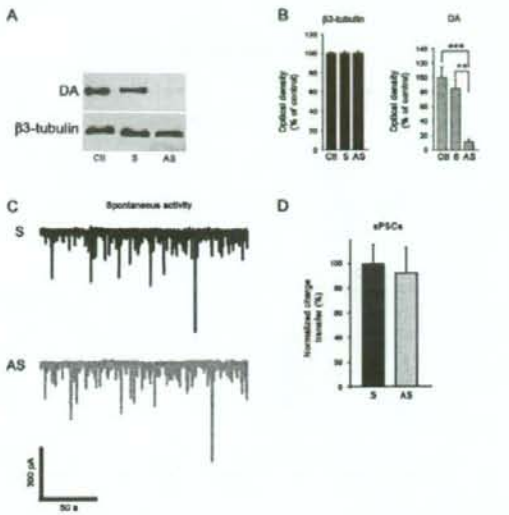

Fig. 6. Effects of DA downregulation on network activity. Mixed hippocampal cultures of 21 DIV treated for 2 days in the absence (untreated) or the presence of 10 µM sense (S) or antisense (AS) oligonucleotides. Following treatment, the cells were either used for western blot analysis (A,B) or electrophysiology recordings (C,D). **P<0.001, Bonferroni's test. (C) Using whole-cell recordings, sPSCs were detected at –60 mV in sense- (black trace) and antisense-treated neurons (gray trace). (D) Histogram showing the sPSC average charge transfer in all recorded neurons.

plaques (Ikeda et al., 1996). It is thus possible that elevated DA levels stabilize actin filaments in spines and alter their dynamic turnover (retraction). This inhibition of spine retraction by DA might lead to the increase in spine density.

In addition, our data show that DA regulates spine shape and size. Indeed, DA-GFP overexpression in mature cultured hippocampal neurons caused elongation of dendritic spines, which were similar to the spines observed in GFP-DA-expressing cortical neurons (Hayashi and Shirao, 1999). Furthermore, DA-GFP increases spine head width. This finding is corroborated by studies showing that downregulation of DA significantly decreases the width of filopodia spines (Takahashi et al., 2006). The morphological changes of dendritic spines induced by DA-GFP are mediated by its actin-binding domain as illustrated by our data (see Fig. 1A-G).

It has been reported that drebrin interacts directly with profilin (Mammoto et al., 1998), an actin-binding protein, known to stimulate actin polymerization (Carlsson et al., 1977; Buss et al., 1992; Rothkegel et al., 1996). One possible mechanism to induce morphological changes of dendritic spines is that DA recruits profilin to stimulate actin polymerization, leading to the elongation and increase in size of dendritic spines.

It has also been shown that DA reduced the movement of actin over a myosin-bound surface in the sliding actin motility assay, and inhibited the actin-based ATPase activity of myosin (Hayashi et al., 1996). The actomyosin-based machinery might thus be another mechanism involved in the elongation of spines. Based on these observations, we suggest that elongation of spines induced by DA-GFP may result from the superimposition of two additive mechanisms: polymerization of actin and inhibition of actomyosin activity and that DA is a key protein in the plasticity of dendritic spines.

DA modulates glutamatergic and GABAergic synaptic transmission

Our data showed that the long protrusions induced by DA are associated with presynaptic glutamatergic terminals. Despite the increased spine density (by about 43%), the density of glutamatergic terminals is not modified. However, the average number of active zone-associated bassoon clusters on spines is increased twice. Since bassoon is a component of the presynaptic apparatus of both excitatory glutamatergic and inhibitory GABAergic synapses (Richter et al., 1999), the increase of bassoon clusters suggests that at least some of the dendritic spines share the same glutamatergic terminal. Consistent with this idea, a single glutamatergic terminal could be contacted by two DA dendritic spines (see arrowheads in Fig. 4). As a result, the density of glutamatergic synapses is increased. Furthermore, our electrophysiological data demonstrate that these synapses are functional and more active. Indeed, an increase in the frequency (~27%) and amplitude (~18%) of mEPSCs were observed in DA-GFP neurons. The frequency increase could result from the augmented number of functional excitatory synapses, whereas the amplitude increase could be due to spine head widening (~13%) and/or to simultaneous glutamate release at multiple active sites. Bath application of glutamatergic agonists showed that overall density of receptors is preserved in DA-GFP neurons. This method does not permit us to distinguish the response mediated by extrasynaptic receptors from that mediated by synaptic receptors.

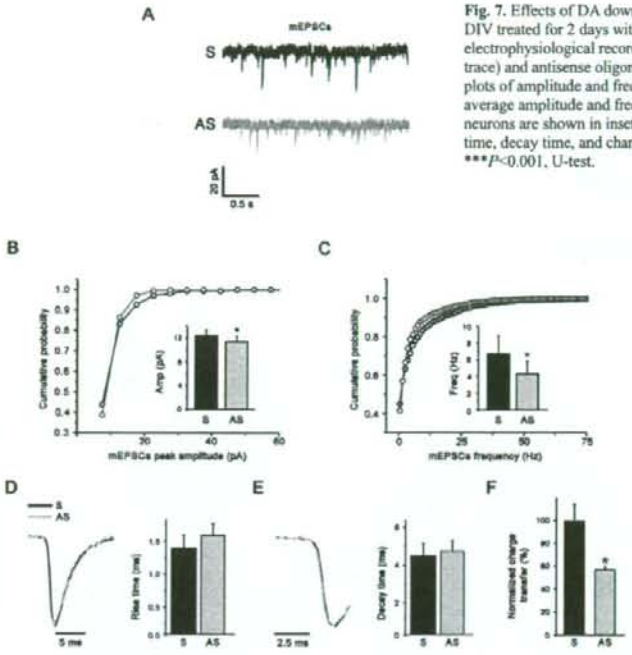

Fig. 7. Effects of DA downregulation on glutamate function. Mixed hippocampal cultures of 21 DIV treated for 2 days with 10 μM sense or antisense oligonucleotides, followed by electrophysiological recording. (A) Examples of mEPSCs recordings from DA sense (black trace) and antisense oligonucleotide-treated neurons (gray trace). (B,C) Cumulative probability plots of amplitude and frequency of mEPSCs in sense- and antisense-treated neurons. The average amplitude and frequency of mEPSCs in sense and antisense oligonucleotide-treated neurons are shown in insets. *P<0.05, K-S test. (D-F) Histograms showing the average rise time, decay time, and charge transfer of mEPSCs in oligonucleotide-treated neurons. ***P<0.001, U-test.

Therefore, these results show that overall density of glutamatergic membrane receptors (extrasynaptic and synaptic) was comparable in both GFP and DA-GFP neurons. Thus, the increased amplitude of mEPSCs could be explained by the spine head widening and the redistribution of glutamatergic extrasynaptic receptors to synaptic sites. The fact that the mEPSC kinetics was comparable in GFP and DA-GFP neurons, suggests that the subunit composition of glutamate receptors was not different in the newly formed and the already established excitatory synapses of DA neurons.

Despite a 43% increase in the density of excitatory synapses in DA-GFP neurons, we did not observe an equivalent increase in mEPSC frequency. This could suggest that synapses on dendritic shafts move on newly formed spines and/or that some of the DA-GFP excitatory synapses are inactive. In both cases, DA-GFP overexpression resulted in a significant increase in excitatory synaptic activity. As a result of the amplitude and frequency changes of mEPSCs in DA-GFP neurons, the glutamatergic transmission efficacy was significantly increased in DA-GFP compared with that of GFP neurons.

Our data revealed that although the mIPSC properties change (frequency, amplitude, and kinetics), the GABAergic transmission efficacy in DA-GFP neurons was not significantly different. The possible mechanisms that mediate the effect of DA on GABA postsynaptic activity are unknown. However it is interesting that DA could interact with gephyrin, a $GABA_A$ receptor anchoring protein (Kneussel and Loebrich, 2007), through profilin (Mammoto et al., 1998). Immunocytochemical data showed that the density of GABA synapses was also similar in GFP and DA-GFP neurons. As a result, the average inhibition to excitation charge transfer ratio is significantly reduced in DA-GFP neurons. Altogether, these observations indicate that DA-GFP overexpression increases the density of excitatory relative to inhibitory synapses, and enhances the excitation to inhibition ratio. The excitatory to inhibitory synapse ratio is believed to be crucial for normal neuronal computation and is generally kept constant by homeostatic mechanisms (Burrone et al., 2002; Hausser et al., 2000; Knott et al., 2002; Liu, 2004; Turrigiano and Nelson, 2004). Some of the factors that control the overall change in the ratio of excitatory-inhibitory synapse number and activity have only recently been discovered. Several studies have implicated the synaptic cell adhesion molecules called neuroligin (NLG) proteins and the scaffolding postsynaptic density protein PSD-95 (Prange et al., 2004; Chih et al., 2005; Levinson et al., 2005; Levinson and El Husseini, 2005a; Levinson and El Husseini, 2005b). An alteration in the excitation-inhibition synaptic balance was also suggested to occur in several neurodevelopmental psychiatric disorders, including autism and some forms of mental retardation (Rubenstein and Merzenich, 2003; Levinson and El Husseini, 2005a; Levinson and El Husseini, 2005b). The importance of our findings is emphasized by the recent discovery that the drebrin level is increased in the superior frontal cortex in neurological disorders accompanied by mild cognitive impairment (MCI) (Counts et al., 2006; Kojima and Shirao, 2007). It has been suggested that this might be a compensatory reaction to the reduced synaptic function in MCI.

Since overexpression of DA affected the glutamate and GABA synaptic properties, we investigated the functional consequences of a reduced DA expression. In DA-knockdown neurons, both amplitude and frequency of mEPSCs were reduced. The decreased amplitude of mEPSCs could be explained by the decreased in the width of filopodia spines observed in DA-knockdown neurons (Takahashi et al., 2006). The decreased frequency of mEPSCs in DA-knockdown neurons could be due to the decreased number of functional excitatory synapses. This possibility is supported by the fact that DA-knockdown neurons displayed a significant decrease in the density of filopodia spines (Takahashi et al., 2003; Takahashi et al., 2006). Similarly to mEPSCs, the frequency and amplitude of mIPSCs were also reduced in DA-knockdown neurons. These decreases could be due to the loss of dendritic spines containing functional inhibitory synapses (see arrows in Fig. 4F). Spines receiving both an excitatory and inhibitory input were first described by Jones and Powell (Jones and Powell, 1969) in the cat somatosensory cortex, and have since been implicated in inhibitory mechanisms by which the inhibitory synapses can reduce the excitatory influence of other synapses (Dehay et al., 1991; Knott et al., 2002). The fact that the kinetics of mEPSCs and mIPSCs were not affected by DA knockdown, suggests that the subunit composition of the glutamate and GABA receptor channels were not different in residual glutamatergic and GABAergic synapses, respectively, of DA-knockdown neurons. The parallel effects

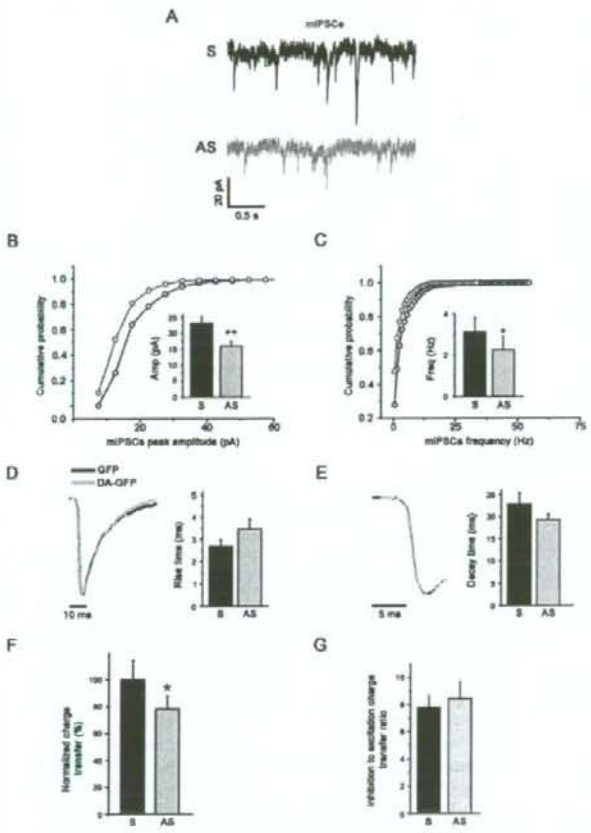

Fig. 8. Effects of DA downregulation on GABA function. Mixed hippocampal cultures of 21 DIV treated for 2 days with 10 μM sense (S) or antisense (AS) DA oligonucleotides, followed by electrophysiological recording. (A) Examples of mIPSC recordings from sense (black trace) and antisense neurons (gray trace). (B,C) Cumulative probability plots of amplitude and frequency of mIPSCs in sense and antisense oligonucleotide-treated neurons. The average amplitude and frequency of mIPSCs in oligonucleotide-treated neurons are shown in insets. *P<0.05, **P<0.01, K-S test. (D-G) Histograms showing the average rise time, decay time, charge transfer and inhibition to excitation charge transfer ratio of mIPSCs in oligonucleotide-treated neurons. ***P<0.001, U-test.

exerted by DA knockdown on mEPSCs and mIPSCs resulted in the reduction of both glutamatergic and GABAergic transmission efficacy. Despite these changes, the inhibition to excitation ratio was not affected by the 73% reduction of DA expression. Combined with the data described above, these results indicated that the residual DA was not sufficient to affect the functional balance between excitation and inhibition. One possible explanation of the effects of DA on the inhibitory to excitatory ratio is that in the case of overexpression of DA we affect only transfected postsynaptic neurons, whereas in the case of underexpression of DA we also affect the presynaptic neurons. Thus, the amounts of DA available can contribute to the homeostatic mechanism that maintains the structural and functional balance between excitatory and inhibitory synapses.

Interestingly, a decreased level in DA content is reported in the superior temporal cortex in MCI and Alzheimer disease (Counts et al., 2006; Kojima and Shirao, 2007). In addition, the level of postsynaptic DA has been shown to strongly correlate with the severity of cognitive impairment (Counts et al., 2006; Kojima and Shirao, 2007). This indicated that a critical level of DA protein might be required for normal function. Therefore, we propose a model in which improper expression of DA might trigger either an imbalance in neuronal excitability or an alteration in synaptic transmission. In both cases, these alterations result in synaptic dysfunction reminiscent of that observed in the cognitive impairment accompanying normal aging and neurological disorders, including Alzheimer disease (Harigaya et al., 1996; Hatanpää et al., 1999; Counts et al., 2006; Kojima and Shirao, 2007) and Down syndrome (Shim and Lubec, 2002).

In conclusion, the identification of factors involved in synaptogenesis should enhance our understanding of the mechanisms responsible for synaptic plasticity as well as the cellular and molecular defects observed in neurological disorders.

Materials and Methods

cDNA constructs

The full-length drebrin A (DA, NCBI accession number NM-031024) fragment was amplified by PCR and inserted into pEGFP-N1 vector (BD Bioscience Clontech, Palo Alto, CA). The DA-GFP construct was subsequently fully sequenced. We also used GFP-ABS and GFP-DAΔABS constructs (see Hayashi et al., 1999).

Cell lines, transfection and immunofluorescence

Chinese Ovary (CHO-K1) cells were obtained from the American Type Tissue Culture Collection (ATCC, Molsheim, France). They were grown in F12 (Invitrogen, Cergy Pontoise, France), supplemented with 10% fetal bovine serum (FBS, Invitrogen), 2 mM glutamine (Invitrogen), 100 U/ml penicillin and 100 mg/ml streptomycin (Sigma, Lyon, France). Cells were rinsed one time with serum-free medium (Opti-MEM, Invitrogen) and transfections were performed according to the manufacturer's protocol (Invitrogen). Briefly, cells were incubated in a solution containing 500 μl Opti-MEM, 4 μl Plus reagent, 6 μl lipofectamine reagent (Invitrogen) and 1 μg of either the GFP, the DA-GFP, the GFP-ABS or the GFP-DAΔABS construct. After incubation for 4 hours at 37°C, the transfection mixture was replaced by a fresh complete growth medium containing 10% FBS. 24 hours after transfection, cells were fixed with 4% paraformaldehyde (PFA) in 0.12 M phosphate buffer (PB), pH 7.2-7.4 for 20 minutes at room temperature (RT).

Quantitative analyses of the number of transfected cells were performed using a fluorescence microscope with a ×20 objective. Twenty fields per coverslip per experiment (n=3) were analyzed. Data were expressed as mean % of total cells per experiment ± s.e.m.

For the F-actin staining, the cells were incubated with 0.5% Triton X-100 and 1% blocking reagent (BR, Roche, Meylan, France) for 30 minutes and exposed for 2 hours at RT to 0.5 U per coverslip of Texas-Red-labeled X phalloidin (Molecular Probes, Leiden, Netherlands), rinsed in PB and incubated with 0.5 μg/ml DNA intercalant Hoechst 33258 (Molecular Probes). Cells were rinsed in PB and then mounted with Fluoromount G (Electron Microscopy, Fort Washington, PA).

In some experimental sets (n=3), the microfilament-depolymerizing drug cytochalasin B (Sigma, used at 10 μg/ml final concentration in 0.1% dimethylsulfoxide) was added into the medium to assess the stability of F-actin of transfected cells. After incubation with cytochalasin B for 10 minutes, cells were fixed with PFA for 20 minutes, washed three times with PB, stained for F-actin as described above, rinsed in PB, then incubated with Hoechst 33258, and mounted with Fluoromount G.

Analysis was performed on a Leica (Mannheim, Germany) TCS SP2 confocal microscope using the 488 nm band of an Ar laser and the 543 nm band of a He-Ne laser for excitation of GFP and Texas Red, respectively. Images were acquired by sequential scanning using ×63 1.32 oil-immersion lens (zoom 3) and processed with Adobe Photoshop. Results are shown in supplementary material Figs S1-S4.

Primary cultures of rat hippocampal neurons and transfection

Mixed hippocampal cultures were prepared from embryonic day 18 (E18) rats according to Rami et al. (Rami et al., 2006). At 21 DIV, mixed hippocampal cultures were transiently transfected using a Magnetofection Kit (OZ Biosciences, Marseille, France) and lipofectamine 2000 reagent according to the OZ Biosciences protocol. Following transfection, the cells were either used for electrophysiology recordings or fixed with 4% PFA in 0.12 M phosphate buffer (PB), pH 7.2-7.4 for 20 minutes at RT for immunofluorescence. The transfection efficiency was less than 1%.

Immunofluorescence

For single immunolabeling of DA and double immunolabeling of DA/synaptophysin and DA/PSD-95, mixed hippocampal cultures of 21 DIV were incubated overnight at RT in DA antiserum (1:500) (Aoki et al., 2005) or a mixture of DA antiserum and either synaptophysin (1:300, Chemicon, Temecula, CA), or PSD-95 (1:500, Upstate, Charlottesville, VA) monoclonal antibodies diluted in PB containing 1% BR. After several rinses in PB, coverslips were incubated in a mixture of Alexa 488-conjugated goat anti-rabbit IgG and Cy3-conjugated goat anti-mouse IgG (1:200, both from Jackson Immunoresearch, West Grove, PA) diluted in PB containing 1% BR.

For double labeling of DA/F-actin, cells were exposed for 2 hours at RT to 0.5 U per coverslip of Texas-Red X phalloidin prepared in PB containing 1% BR.

Single immunolabeling of bassoon, double immunolabeling of synaptophysin/β2,3 or Gad-65/vGlut1 were performed on hippocampal neurons transfected with GFP or DA-GFP. Cells were incubated with the following primary antibodies (most from Chemicon): polyclonal synaptophysin (1:500) and mouse monoclonal antibody against $GABA_A$ receptor beta chain (β2,3, 1:500) or mouse monoclonal antibody against Gad 65 (one of the glutamic acid decarboxylase isoforms, 1:300) and guinea pig polyclonal antiserum against vGlut1 (vesicular glutamate transporter 1, 1:5000) or mouse monoclonal antibody against bassoon (1:300, Assay designs, Ann Arbor, MI). After several rinses in PB, coverslips were incubated for 1 hour at RT in biotinylated goat- anti-rabbit IgG (1:200) or anti-mouse IgG (1:200), and then incubated in a mixture of Cy5-conjugated streptavidin and Cy3-conjugated goat anti-mouse IgG or Cy3-conjugated donkey anti-guinea pig IgG (1:200, all from Jackson Immunoresearch). Bassoon staining was revealed with Alexa Fluor 594-conjugated goat anti-mouse IgG (1:200, Molecular Probes) diluted in PB containing 1% BR. In all cases, no labeling was detected when specific antibodies were replaced with normal rabbit, mouse, guinea pig serum or when primary antibodies were omitted.

Image acquisition and quantification

All measurements were performed on spiny and pyramidal neurons that were visually identified based on their morphology (Benson et al., 1994). Images were acquired with an Olympus fluoview-500 confocal microscope (Olympus, France) using an oil immersion ×60 1.4 lens (zoom 3). Dendritic protrusions were reconstructed from 7 to 15 serial images of 0.5 μm thickness projected onto one plane. For morphometric analysis, protrusion length, width and density were measured from projected images using Neurolucida software as described previously (Rami et al., 2006).

Analysis of synaptic proteins was performed with an Olympus Fluoview-500 confocal microscope using the 488, 543, 633 laser lines for excitation of GFP, Cy3 and Cy5, respectively. For quantitation of synaptic protein clusters, pictures from GFP and DA-GFP neurons were taken sequentially using ×63 1.4 (zoom 3) with the same exposure parameters. Then the projections of z-stacks were thresholded equally to eliminate the background of dendritic staining and the remaining clusters were counted based on their location either on dendritic shafts or on dendritic protrusions using Neurolucida or ImageJ softwares. Five to ten transfected neurons were chosen randomly from three independent experiments for GFP and DA-GFP constructs and the number of clusters was collected from at least three dendritic segments of 100 μm per neuron. Then, the density of the synaptic protein clusters was determined similarly to protrusion density.

Westerns blot analysis

For western blot analysis, cultures were homogenized in 50 mM Tris-HCl, pH 6.8, 5% SDS, 6% 2-mercaptoethanol, 10% glycerol and 4 mM EDTA. Protein samples were boiled for 10 minutes, and equal amounts were loaded into each well, resolved on 8% SDS-polyacrylamide gels and transferred onto Hybond-ECL nitrocellulose membranes (Amersham Biosciences, Germany). Blots were then blocked, immunostained with appropriate antibodies and immunodetected using the enhance chemiluminescence system (ECL, Amersham Biosciences). Chemiluminescent signals were projected on X-ray film and digitalized, and the signals were quantified using ImageJ.

Antisense experiments

Translation of DA was suppressed by treatment of cultures with an antisense phosphorothioate-substituted DNA oligonucleotides (AS) (Takahashi et al., 2006). The sense phosphorothioate oligonucleotide (S) (Takahashi et al., 2006) was used as negative control since the sense oligo treatment has no effect on the expression of DA, β3-tubulin and synaptic activity compared with untreated cultures (supplementary material Fig. S4). Therefore, we used sense oligo-treated neurons for the analysis of the control neuronal activity. At 21 DIV, cultures were treated for 2 days in the absence (untreated) or the presence of 10 μM sense or antisense oligonucleotides. Following treatment, the cells were either used for western blot analysis or electrophysiology recordings.

Whole-cell recording

sPSCs or mPSCs were recorded from visually identified spiny and pyramidal neurons (Chudotvorova et al., 2005; Rami et al., 2006). The mEPSCs or mIPSCs were isolated at –60 mV in the presence of TTX, D-AP5, strychnine and bicuculline/CNQX. We took into account for analysis, only neurons in which both mEPSCs and mIPSCs were recorded. To evaluate the change produced by DA-GFP overexpression or by treatment with antisense oligonucleotides against DA on network activity and the overall synaptic strength of a single neuron (Turrigiano et al., 1998; Burrone et al., 2002; Liu, 2004; Chih et al., 2005), the mean charge transfer was determined. This parameter depends simultaneously on the amplitude, frequency and kinetic of postsynaptic currents. Therefore, during spontaneous activity, charge transfer reflects neuronal network activity. When this activity is blocked by TTX, the charge transfer reflects the overall synaptic strength of a single neuron (Liu, 2004). Charge transfers for sPSCs or mPSCs were calculated for each recorded neuron as the sPSCs or mPSCs area (charge transferred by single postsynaptic current) multiplied on instantaneous frequency value (instantaneous frequency=1/inter-event interval). In each experiment, the mean charge transfer values were normalized relative to the average mean control value (expressed in %). To evaluate the effects of postsynaptic receptor agonists within different cells, the current densities (amplitude/cell capacitance) were compared. Amplitudes of currents induced by bath application of agonists were measured 10 seconds after starting perfusion with agonist containing solution (see Fig. 4A).

Statistical analysis

All experiments were repeated at least three times with different culture series. Morphological, immunostaining and western blot data were statistically analyzed by unpaired Student's *t*-test for comparing two groups, or by ANOVA, with *a* post hoc Bonferroni's *t*-test (Bonferroni test) for multiple comparison, as applicable.

Statistical analyses for frequency, amplitude, and area of mPSCs were performed with the nonparametric Kolmogorov-Smirnov (K-S) test. Unpaired Student's *t*-test was used to examine the statistical significance of the differences between groups of others parameters (decay time, rise time, density of agonist induced current). All data parameters were expressed as the mean ± s.e.m. To determine the difference between groups of charge transfer data, Kolmogorov-Smirnov as well as Mann-Whitney U (U-test) tests were used; the higher value of P was taken into account.

We thank Djaffar Boussa, Santiago Rivera, François Feron and Michel Khrestchatisky for critical reading of the manuscript. We also thank Marie-Pierre Blanchard for her help with the Leica laser microscope. This work was supported by grants from the Institut National de la Santé et de la Recherche Médicale (INSERM) and the Centre National de la Recherche Scientifique (CNRS). This project was initiated in the INMED laboratory directed by Yezekiel Ben Ari.

References

Aoki, C., Sekino, Y., Hanamura, K., Fujisawa, S., Mahadomrongkul, V., Ren, Y. and Shirao, T. (2005). Drebrin A is a postsynaptic protein that localizes in vivo to the submembranous surface of dendritic sites forming excitatory synapses. *J. Comp. Neurol.* **483**, 383-402.

Ballestrem, C., Wehrle-Haller, B. and Imhof, B. A. (1998). Actin dynamics in living mammalian cells. *J. Cell Sci.* **111**, 1649-1658.

Benson, D. L., Watkins, F. H., Steward, O. and Banker, G. (1994). Characterization of GABAergic neurons in hippocampal cell cultures. *J. Neurocytol.* **23**, 279-295.

Burrone, J., O'Byrne, M. and Murthy, V. N. (2002). Multiple forms of synaptic plasticity triggered by selective suppression of activity in individual neurons. *Nature* **420**, 414-418.

Buss, F., Temm-Grove, C., Henning, S. and Jockusch, B. M. (1992). Distribution of profilin in fibroblasts correlates with the presence of highly dynamic actin filaments. *Cell Motil. Cytoskeleton* **22**, 51-61.

Carlsson, L., Nystrom, L. E., Sundkvist, I., Markey, F. and Lindberg, U. (1977). Actin polymerizability is influenced by profilin, a low molecular weight protein in non-muscle cells. *J. Mol. Biol.* **115**, 465-483.

Chih, B., Engelman, H. and Scheiffele, P. (2005). Control of excitatory and inhibitory synapse formation by neuroligins. *Science* **307**, 1324-1328.

Chudotvorova, I., Ivanov, A., Rama, S., Hübner, C. A., Pellegrino, C., Ben-Ari, Y. and Medina, I. (2005). Early expression of KCC2 in rat hippocampal cultures augments expression of functional GABA synapses. *J. Physiol.* **566**, 671-679.

Cooper, J. A. (1987). Effects of cytochalasin and phalloidin on actin. *J. Cell Biol.* **105**, 1473-1478.

Counts, S. E., Nadeem, M., Lad, S. P., Wuu, J. and Mufson, E. J. (2006). Differential expression of synaptic proteins in the frontal and temporal cortex of elderly subjects with mild cognitive impairment. *J. Neuropathol. Exp. Neurol.* **65**, 592-601.

Dehay, C., Douglas, R. J., Martin, K. A. and Nelson, C. (1991). Excitation by geniculocortical synapses is not 'vetoed' at the level of dendritic spines in cat visual cortex. *J. Physiol.* **440**, 723-734.

Edson, K., Weisshaar, B. and Matus, A. (1993). Actin depolymerisation induces process formation on MAP2-transfected non-neuronal cells. *Development* **117**, 689-700.
Fifkova, E. and Delay, R. J. (1982). Cytoplasmic actin in neuronal processes as a possible mediator of synaptic plasticity. *J. Cell Biol.* **95**, 345-350.
Fukazawa, Y., Saitoh, Y., Ozawa, F., Ohta, Y., Mizuno, K. and Inokuchi, K. (2003). Hippocampal LTP is accompanied by enhanced F-actin content within the dendritic spine that is essential for late LTP maintenance *in vivo*. *Neuron* **38**, 447-460.
Harigaya, Y., Shoji, M., Shirao, T. and Hirai, S. (1996). Disappearance of actin-binding protein, drebrin, from hippocampal synapses in Alzheimer's disease. *J. Neurosci. Res.* **43**, 87-92.
Harris, K. M. and Kater, S. B. (1994). Dendritic spines: cellular specializations imparting both stability and flexibility to synaptic function. *Annu. Rev. Neurosci.* **17**, 341-371.
Hatanpaa, K., Isaacs, K. R., Shirao, T., Brady, D. R. and Rapoport, S. I. (1999). Loss of proteins regulating synaptic plasticity in normal aging of the human brain and in Alzheimer disease. *J. Neuropathol. Exp. Neurol.* **58**, 637-643.
Hausser, M., Spruston, N. and Stuart, G. J. (2000). Diversity and dynamics of dendritic signaling. *Science* **290**, 739-744.
Hayashi, K. and Shirao, T. (1999). Change in the shape of dendritic spines caused by overexpression of drebrin in cultured cortical neurons. *J. Neurosci.* **19**, 3918-3925.
Hayashi, K., Ishikawa, R., Ye, L. H., He, X. L., Takata, K., Kohama, K. and Shirao, T. (1996). Modulatory role of drebrin on the cytoskeleton within dendritic spines in the rat cerebral cortex. *J. Neurosci.* **16**, 7161-7170.
Hayashi, K., Ishikawa, R., Kawai-Hirai, R., Takagi, T., Taketomi, A. and Shirao, T. (1999). Domain analysis of the actin-binding and actin-remodeling activities of drebrin. *Exp. Cell Res.* **253**, 673-680.
Ikeda, K., Kaub, P. A., Asada, H., Uyemura, K., Toya, S. and Shirao, T. (1996). Stabilization of adhesion plaques by the expression of drebrin A in fibroblasts. *Brain Res. Dev. Brain Res.* **91**, 227-236.
Ishikawa, R., Hayashi, K., Shirao, T., Xue, Y., Takagi, T., Sasaki, Y. and Kohama, K. (1994). Drebrin, a development-associated brain protein from rat embryo, causes the dissociation of tropomyosin from actin filaments. *J. Biol. Chem.* **269**, 29928-29933.
Ishikawa, R., Katoh, K., Takahashi, A., Xie, C., Oseki, K., Watanabe, M., Igarashi, M., Nakamura, A. and Kohama, K. (2007). Drebrin attenuates the interaction between actin and myosin-V. *Biochem. Biophys. Res. Commun.* **359**, 398-401.
Jones, E. G. and Powell, T. P. (1969). Morphological variations in the dendritic spines of the neocortex. *J. Cell Sci.* **5**, 509-529.
Kneussel, M. and Loebrich, S. (2007). Trafficking and synaptic anchoring of ionotropic inhibitory neurotransmitter receptors. *Biol. Cell* **99**, 297-309.
Knott, G. W., Quairiaux, C., Genoud, C. and Welker, E. (2002). Formation of dendritic spines with GABAergic synapses induced by whisker stimulation in adult mice. *Neuron* **34**, 265-273.
Kojima, N. and Shirao, T. (2007). Synaptic dysfunction and disruption of postsynaptic drebrin-actin complex: a study of neurological disorders accompanied by cognitive deficits. *Neurosci. Res.* **58**, 1-5.
Levinson, J. N. and El-Husseini, A. (2005a). Building excitatory and inhibitory synapses: balancing neuroligin partnerships. *Neuron* **48**, 171-174.
Levinson, J. N. and El-Husseini, A. (2005b). New players tip the scales in the balance between excitatory and inhibitory synapses. *Mol. Pain* **1**, 12.
Levinson, J. N., Chery, N., Huang, K., Wong, T. P., Gerrow, K., Kang, R., Prange, O., Wang, Y. T. and El-Husseini, A. (2005). Neuroligins mediate excitatory and inhibitory synapse formation: involvement of PSD-95 and neurexin-1beta in neuroligin-induced synaptic specificity. *J. Biol. Chem.* **280**, 17312-17319.
Liu, G. (2004). Local structural balance and functional interaction of excitatory and inhibitory synapses in hippocampal dendrites. *Nat. Neurosci.* **7**, 373-379.
Mammoto, A., Sasaki, T., Asakura, T., Hotta, I., Imamura, H., Takahashi, K., Matsuura, Y., Shirao, T. and Takai, Y. (1998). Interactions of drebrin and gephyrin with profilin. *Biochem. Biophys. Res. Commun.* **243**, 86-89.
Matus, A. (2000). Actin-based plasticity in dendritic spines. *Science* **290**, 754-758.
Matus, A., Ackermann, M., Pehling, G., Byers, H. R. and Fujiwara, K. (1982). High actin concentrations in brain dendritic spines and postsynaptic densities. *Proc. Natl. Acad. Sci. USA* **79**, 7590-7594.
McKernan, R. M. and Whiting, P. J. (1996). Which GABAA-receptor subtypes really occur in the brain? *Trends Neurosci.* **19**, 139-143.
Papa, M., Bundman, M. C., Greenberger, V. and Segal, M. (1995). Morphological analysis of dendritic spine development in primary cultures of hippocampal neurons. *J. Neurosci.* **15**, 1-11.
Prange, O., Wong, T. P., Gerrow, K., Wang, Y. T. and El-Husseini, A. (2004). A balance between excitatory and inhibitory synapses is controlled by PSD-95 and neuroligin. *Proc. Natl. Acad. Sci. USA* **101**, 13915-13920.
Rami, G., Caillard, O., Medina, I., Pellegrino, C., Fattoum, A., Ben-Ari, Y. and Ferhat, L. (2006). Change in the shape and density of dendritic spines caused by overexpression of acidic calponin in cultured hippocampal neurons. *Hippocampus* **16**, 183-197.
Richter, K., Langnaese, K., Kreutz, M. R., Olias, G., Zhai, R., Scheich, H., Garner, C. C. and Gundelfinger, E. D. (1999). Presynaptic cytomatrix protein bassoon is localized at both excitatory and inhibitory synapses of rat brain. *J. Comp. Neurol.* **408**, 437-448.
Rothkegel, M., Mayboroda, O., Rohde, M., Wucherpfennig, C., Valenta, R. and Jockusch, B. M. (1996). Plant and animal profilins are functionally equivalent and stabilize microfilaments in living animal cells. *J. Cell Sci.* **109**, 83-90.
Rubenstein, J. L. and Merzenich, M. M. (2003). Model of autism: increased ratio of excitation/inhibition in key neural systems. *Genes Brain Behav.* **2**, 255-267.
Sasaki, Y., Hayashi, K., Shirao, T., Ishikawa, R. and Kohama, K. (1996). Inhibition by drebrin of the actin-bundling activity of brain fascin, a protein localized in filopodia of growth cones. *J. Neurochem.* **66**, 980-988.
Sekino, Y., Kojima, N. and Shirao, T. (2007). Role of actin cytoskeleton in dendritic spine morphogenesis. *Neurochem. Int.* **51**, 92-104.
Shim, K. S. and Lubec, G. (2002). Drebrin, a dendritic spine protein, is manifold decreased in brains of patients with Alzheimer's disease and Down syndrome. *Neurosci. Lett.* **324**, 209-212.
Shirao, T., Hayashi, K., Ishikawa, R., Isa, K., Asada, H., Ikeda, K. and Uyemura, K. (1994). Formation of thick, curving bundles of actin by drebrin A expressed in fibroblasts. *Exp. Cell Res.* **215**, 145-153.
Takahashi, H., Sekino, Y., Tanaka, S., Mizui, T., Kishi, S. and Shirao, T. (2003). Drebrin-dependent actin clustering in dendritic filopodia governs synaptic targeting of postsynaptic density-95 and dendritic spine morphogenesis. *J. Neurosci.* **23**, 6586-6595.
Takahashi, H., Mizui, T. and Shirao, T. (2006). Down-regulation of drebrin A expression suppresses synaptic targeting of NMDA receptors in developing hippocampal neurones. *J. Neurochem.* **97 Suppl. 1**, 110-115.
Turrigiano, G. G. and Nelson, S. B. (2004). Homeostatic plasticity in the developing nervous system. *Nat. Rev Neurosci* **5**, 97-107.
Turrigiano, G. G., Leslie, K. R., Desai, N. S., Rutherford, L. C. and Nelson, S. B. (1998). Activity-dependent scaling of quantal amplitude in neocortical neurons. *Nature* **391**, 892-896.
Yahara, I., Harada, F., Sekita, S., Yoshihira, K. and Natori, S. (1982). Correlation between effects of 24 different cytochalasins on cellular structures and cellular events and those on actin *in vitro*. *J. Cell Biol.* **92**, 69-78.
Yuste, R. and Bonhoeffer, T. (2001). Morphological changes in dendritic spines associated with long-term synaptic plasticity. *Annu. Rev. Neurosci.* **24**, 1071-1089.

Cerebral Cortex February 2008;18:315-330
doi:10.1093/cercor/bhm056
Advance Access publication May 20, 2007

Quantitative Chemical Composition of Cortical GABAergic Neurons Revealed in Transgenic Venus-Expressing Rats

Masakazu Uematsu[1,2,3], Yasuharu Hirai[4,5], Fuyuki Karube[4], Satoe Ebihara[1], Megumi Kato[6], Kuniya Abe[7], Kunihiko Obata[1,8], Sachiko Yoshida[2], Masumi Hirabayashi[5,6], Yuchio Yanagawa[1,3,9] and Yasuo Kawaguchi[4,5]

[1]Laboratory of Neurochemistry, National Institute for Physiological Sciences (NIPS), Okazaki 444-8585, Japan, [2]Department of Materials Science, Toyohashi University of Technology, Toyohashi 441-8580, Japan, [3]SORST, JST, Kawaguchi 332-0012, Japan, [4]Division of Cerebral Circuitry, NIPS, [5]Department of Physiological Sciences, The Graduate University for Advanced Studies (SOKENDAI), Okazaki 444-8585, Japan, [6]Center for Genetic Analysis of Behavior, NIPS, [7]BioResource Center, RIKEN Tsukuba Institute, Tsukuba 305-0074, Japan, [8]Neuronal Circuit Mechanisms Research Group, BSI, RIKEN, Wako 351-0198, Japan and [9]Department of Genetic and Behavioral Neuroscience, Gunma University Graduate School of Medicine, Maebashi 371-8511, Japan

The first 2 authors contributed equally to this work.

Although neocortical GABAergic (γ-aminobutyric acidergic) interneurons have been the focus of intense study, especially in the rat, a consensus view of the functional diversity and organization of inhibitory cortical neurons has not yet been achieved. To better analyze GABAergic neurons in the rat, we used a bacterial artificial chromosome (BAC) construct and established 2 lines of transgenic rats that coexpress Venus, a yellow fluorescent protein, with the vesicular GABA transporter. The brain GABA content from both transgenic lines was similar to the level found in wild-type rats. In the frontal cortex, Venus was expressed in >95% of GABAergic neurons, most of which also expressed at least one of 6 biochemical markers, including α-actitin-2, which preferentially labeled late-spiking neurogliaform cells. Taking advantage of the fact that Venus expression allows for targeted recording from all classes of nonpyramidal cells, irrespective of their somatic morphologies, we demonstrated that fast-spiking neurons, which were heterogeneous in somatic size as well as vertical dendritic projection, had relatively uniform horizontal dimensions, suggesting a cell type–specific columnar input territory. Our data demonstrate the benefits of VGAT-Venus rats for investigating GABAergic circuits, as well as the feasibility of using BAC technology in rats to label subsets of specific, genetically defined neurons.

Keywords: bacterial artificial chromosome, cortex, interneuron, transgenic rat, Venus, vesicular GABA transporter

Introduction

Inhibitory neurons in the central nervous system (CNS) are diverse in their morphological and physiological characteristics (Somogyi et al. 1998). To explore the functional diversity of cortical interneurons in the rat neocortex, numerous studies have investigated various aspects of these neurons, such as their axonal and dendritic morphologies, chemical expression patterns, firing patterns, and synaptic connectivity (Kawaguchi and Kubota 1997; Gupta et al. 2000; Kawaguchi and Kondo 2002; Markram et al. 2004; Somogyi and Klausberger 2005; Kubota et al. 2007). However, the implications of the data have been hotly debated, and a consensus view on how these neurons can best be functionally classified has not yet been achieved (Nelson 2002; Yuste 2005). Because the expression of several peptides and calcium-binding proteins is correlated with their physiological and morphological characteristics (Kawaguchi and Kubota 1993; Cauli et al. 2000; Wang et al. 2002; Toledo-Rodriguez et al. 2004; Sugino et al. 2006), as well as their differential response to neuromodulators such as acetylcholine and serotonin (Kawaguchi 1997; Porter et al. 1999; Ferezou et al. 2002; Gulledge et al. 2007), their expression can be used to identify functional subclasses of cortical interneurons. However, it has not yet been determined if these chemical markers identify the entire GABAergic cell population in the neocortex. On the other hand, traditional methods of examining nonpyramidal neurons via intracellular recording may sometimes fail to identify GABAergic (γ-aminobutyric acidergic) cell subtypes that are morphologically and/or physiologically similar to pyramidal neurons. Therefore, selective fluorescent labeling of the entire GABAergic cell population in the rat neocortex would greatly advance the analysis of their cellular and circuit organizations.

To date, transgenic labeling of inhibitory cells in mice has utilized green fluorescent protein (GFP) controlled by the promoter of the biosynthetic enzyme for GABA, glutamate decarboxylase (GAD). In these mice, however, GFP expression was restricted to subsets of GABAergic neurons (Oliva et al. 2000; Chattopadhyaya et al. 2004; Lopez-Bendito et al. 2004; Ma et al. 2006). In GAD67-GFP knock-in mice, the overall GABA content was shown to be reduced following destruction of the endogenous GAD67 gene (Tamamaki et al. 2003). Bacterial artificial chromosome (BAC) technology has gradually come to be regarded as a potent method to identify and manipulate specific neuron types in mice (Heintz 2001; Meyer et al. 2002), but its application in rats has not previously been reported. In this study we have, for the first time, produced transgenic rats that have both fluorescent labeling of nearly all cortical GABAergic cells and normal levels of GABA synthesis, thus facilitating the study of GABAergic neurons in tissue that is otherwise physiologically normal. To do this we used a BAC containing 2 genes: one for VGAT, which is responsible for transporting GABA into synaptic vesicles (Ebihara et al. 2003), and another for Venus, a fluorescent marker much brighter than

eGFP (Nagai et al. 2002). This manipulation generated 2 lines of VGAT-Venus transgenic rats from the same BAC construct. We show that in at least one of the 2 lines, GABAergic cells in individual areas in the forebrain are selectively labeled with Venus. In the cerebral cortex almost all Venus-expressing cells in both lines were positive for GABA, and the vast majority expressed at least one of 6 chemical markers used to classify cortical interneurons. Venus labeling facilitated the identification of GABAergic cells and made possible targeted recording of the interneurons with morphological features typical of pyramidal cells.

Materials and Methods

Identification of a Suitable BAC Clone

A BAC clone (#160L22) from a 129SV mouse genomic BAC library (Genome System, St Louis, MO), containing the VGAT gene was identified by PCR as previously described (Ebihara et al. 2003). We determined the nucleotide sequences of the 5′- and 3′-termini of the DNA inserted into the BAC vector and compared their sequences with the EMBL database (accession number AL663091). The comparison revealed that BAC clone #160L22 contains the entire VGAT gene, with an additional 102 and 25 kb of DNA flanking the 5′ end of exon 1 and the 3′ end of exon 3, respectively.

Modification of the BAC Clone

pCS2-Venus, which contains Venus complementary DNA (cDNA) followed by the SV40 polyadenylation signals, was generously provided by Dr A. Miyawaki (RIKEN, Wako, Japan) (Nagai et al. 2002). pKOV-Kan and pDF25 plasmids were a generous gift from Dr M. D. Lalioti (University of Birmingham, Birmingham, UK).

The multiple cloning site following the SV40 polyadenylation signals of pCS2-Venus was changed to a *Not*I-*Nco*I-*Apa*I site by ligation of a synthetic linker to pCS2-Venus digested with *Not*I and *Apa*I, and the resultant plasmid was named pCS2-Venus-N. A 3.6-kb *Eco*RI fragment containing the 5′-flanking region, exon 1 and part of intron 1 of the mouse VGAT (mVGAT) gene was subcloned into pBluescript II (Stratagene, LaJolla, CA) from a BAC clone encoding the mVGAT gene (Ebihara et al. 2003), and the resultant plasmid was named pBS-VGAT-E1. A 1.0-kb *Nco*I fragment containing the Venus cDNA followed by the SV40 polyadenylation signals (poly-A) was excised from pCS2-Venus-N and inserted into pBS-VGAT-E1 digested with *Nco*I in order to place the Venus cDNA in frame into the ATG translational initiation codon of exon 1 of the VGAT gene. This plasmid was named pBS-VGAT-E1-Venus. The multiple cloning site of pBluescript II was changed to a *Sal*I-*Eco*RI-*Nhe*I-*Bam*HI site by ligation of a synthetic linker to pBluescriptII digested with *Sal*I and *Bam*HI, and the resultant plasmid was named pBS-SENB. A 3.3-kb *Eco*RI/*Nhe*I fragment was excised from pBS-VGAT-E1-Venus and inserted into pBS-SENB, and the resultant plasmid was named pBS-VGAT-EN-Venus. The cloning site of pKOV-Kan was changed to a *Sal*I-*Eco*RI-*Nhe*I-*Bam*HI site by ligation of a synthetic linker to pKOV-Kan digested with *Sal*I and *Bam*HI, and the resultant plasmid was named pKOV-SENB. A 3.3-kb *Eco*RI/*Nhe*I fragment was excised from pBS-VGAT-EN-Venus and inserted into pKOV-SENB, and the resultant plasmid was named pKOV-VGAT-Venus. The shuttle vector pKOV-VGAT-Venus contains the Venus cDNA and SV40 poly-A flanked by 2 homologous regions: one is genomic DNA homologous to 941 bp (*Nhe*I/*Nco*I) upstream of the translation initiation site of exon 1 of the VGAT gene and the other is genomic DNA homologous to 1393 bp (*Nco*I/*Eco*RI) downstream of the VGAT gene.

BAC recombinations were performed according to the methods described by Lalioti and Heath (2001). Venus-modified BAC clones were confirmed by PCR, pulse field gel electrophoresis, and Southern blotting.

Generation of BAC Transgenic Rats

For pronuclear injections, BAC DNA was purified with a NucleoBond BAC100 kit (Macherey-Nagel, Düren, Germany) and digested with *Nru*I to release the VGAT-Venus DNA, which consisted of the entire insert of genomic DNA and part of the vector DNA from the BAC backbone. The 133-kb linearized BAC DNA fragment was purified using pulse field gel electrophoresis, dissolved at a concentration of 3 ng/μL in 10 mM TrisCl and 0.1 mM ethylenediaminetetraacetic acid, and then stored at 4 °C. The purified and stored BAC DNA was injected into fertilized eggs of Crlj:Wistar rats (Charles River Japan, Inc., Kanagawa, Japan) according to the procedure described by Takahashi et al. (1999).

Among 318 oocytes injected, 182 could be transferred into pseudopregnant female rats. From them, 25 rats were born. Two transgenic founders were identified from 21 pups by PCR for the presence of Venus. Primers used for the PCR were Venus-F: 5′-ATGGTGAGCAAGGGCGAGGAGCTGT-3′ and Venus-R: 5′-TTACTTGTACAGCTCGTCCATGCCGA-3′. The lines derived from these 2 founders were expanded for further analysis. Venus expression in both lines of newborn rat brains was detected by fluorescence microscopy.

Measurement of GABA Content

Samples from rat brains were homogenized with 0.1 M perchloric acid to extract amino acids and precipitate proteins. The homogenates were centrifuged at 6000 × *g* for 15 min at 4 °C and then the supernatant was neutralized with 0.1 M sodium carbonate. After addition of sodium carbonate, the samples were filtered by using Ultrafree-MC (Millipore Corp., Bedford, MA). Amino acids in the samples were derivatized with *o*-phthalaldehyde/2-mercaptoethanol reagent, and GABA concentrations were measured by using high performance liquid chromatography (BAS, Tokyo, Japan) and fluorescence detection. Protein concentrations were determined using bicinchoninic acid protein assay reagent (Pierce, Rockford, IL), with bovine serum albumin (BSA) as a standard.

Antibodies

Venus was immunohistochemically detected using a rabbit antiserum against eGFP (1: 2000; kind gift from Dr Nobuaki Tamamaki, Kumamoto University). In the cortex of transgenic rats, Venus fluorescence almost always colocalized with the immunofluorescence by its antibody. For GABA immunohistochemistry, a mouse monoclonal antibody was used (1:500; Chemicon [Temecula, CA] MAB316).

Parvalbumin was visualized by a mouse monoclonal antibody (Sigma [Saint Louis, MO] P-3171; 1:2000) and a rabbit antiserum (Swant, Bellinzona, Switzerland PV-28; 1:4000). Somatostatin was immunohistochemically detected by a rabbit antiserum (antisomatostatin 28; Dr Robert Benoit, S 309; 1:4000) or a rat monoclonal antibody against somatostatin (Chemicon, MAB354; 1:250). Calretinin was detected by a mouse monoclonal antibody (Chemicon, MAB1568; 1:4000) or a rabbit antiserum (Swant, 7699/4; 1:2000, Diasorin, Stillwater, MN). Cholecystokinin (CCK) immunoreactivity was detected by a monoclonal antibody raised against CCK/Gastrin (#28.2 MoAb, CURE/UCLA/DDC Antibody/RIA Core; 1:4000) or a rabbit antiserum against CCK-8 (Sigma, C-2581; 1:1000). These 2 antibodies against the same antigens stained the same populations of cells in the rat frontal cortex. Vasoactive intestinal polypeptide (VIP) was immunohistochemically found by a rabbit antiserum (Diasorin, 20077; 1:2000). Calbindin immunoreaction was done by a rabbit antiserum (anticalbindin D; Dr Piers C. Emson; 1:2000).

The expression pattern of α-actinin-2 was investigated using a rabbit specific antiserum against α-actinin-2 (4B2; kind gift from Dr Alan H. Beggs, Children's Hospital Boston; 1:2000) (Wyszynski et al. 1998) or a mouse monoclonal antibody against α-actinin-2 and -3 (EA53; Sigma, A7811; 1:2000). Because α-actinin-3 is not expressed in the brain, the EA53 antibody should be specific for α-actinin-2 in rat brain (Wyszynski et al. 1998). This was confirmed using double immunofluorescence showing the rabbit antiserum and the monoclonal antibody against α-actinin-2 stain the same population of cells in the rat cortex.

Immunohistochemistry in Perfusion-Fixed Brains

After anesthesia with an overdose of Nembutal, transgenic and wild-type Wistar rats (28–32 days postnatal) were perfused through the heart with 10 mL of a solution of 250 mM sucrose, 5 mM $MgCl_2$ in 0.02 M phosphate buffer (pH 7.4) (PB), followed by 200 mL of fixative containing 4% paraformaldehyde, 0.05% glutaraldehyde, and 0.2% picric acid in 0.1 M PB. For GABA immunohistochemistry, the glutaraldehyde concentration was increased to 0.5%. The brains were then removed and postfixed in the same fixative for 2 h.

For the immunoperoxidase reaction, the brains were cut at thickness of 50 μm by a vibrating slicer, to the frontal, parasagittal, or oblique horizontal (parallel to the rhinal fissure) sections. Sections were incubated with 1% H_2O_2 in PB to suppress intrinsic peroxidase activity. Sections were

incubated overnight in the primary antiserum in 0.05 M Tris-HCl buffered saline (pH 7.6) (TBS) containing 10% normal goat serum (NGS), 2% BSA, and 0.5% TritonX-100 (TX). After washes with TBS, the sections were incubated with biotinylated secondary antiserum (Vector Laboratories [Burlingame, CA] 1: 100) in TBS containing 10% NGS, 2% BSA and 0.5% TX. After additional washes, they were incubated in ABC complex in TBS (1: 100; Vector). After incubation with 0.05 M Tris-HCl buffer (TB), the sections were reacted with 3,3'-diamino-benzidine tetrahydrochloride (DAB) and H_2O_2. After washing in PB, the sections were put on gelatin-coated slides and dried. After further treatment with 0.1% OsO_4, in PB, they were dehydrated and coverslipped with Entellan.

Colocalization between Venus and a substance or pairs of substances was investigated using immunofluorescence with cryostat sections. Fixed brains were put in 15% sucrose in PB overnight followed by 30% sucrose in PB overnight before sectioning on a cryostat. The sections were put on a cryostat and sectioned at thickness of 2 μm for GABA immunohistochemistry and 4 μm for other chemical markers.

For combined single immunofluorescence and Venus observation, sections were washed in TBS and then incubated with a primary antibody in TBS containing 10% NGS, 2% BSA, and 0.5% TX overnight. After washes with TBS, the sections were incubated with an Alexa 594-conjugated secondary antibody (1:200; Molecular Probes, Eugene, OR). For experiments using double immunofluorescence for α-actinin-2 and other markers in wild-type rats, sections were incubated with mouse and rabbit primary antibodies, followed by a mixture of Alexa 488- and Alexa 594-conjugated secondary antibodies. After washing in TBS the sections were mounted on gelatin-coated glass slides and dried. The sections were coverslipped with 50% glycerin in TBS and observed by epifluorescence. Cross-reactivity of the secondary antisera used for dual immunofluorescence was tested by incubating control sections first with a single primary antiserum or monoclonal antibody and then with a secondary antibody appropriate for the different primary applied for double staining.

The following filters were used for fluorescence observation: excitation, 485–515 nm; emission, 525–555 nm for Venus; excitation, 545–580 nm; emission, 610 nm for Alexa 594; excitation, 360–370 nm; emission, 420–460 nm for Alexa 350. Peak absorption and emission of Venus are 515 and 528 nm, respectively (Nagai et al. 2002).

Single- and dual-labeled fluorescent cells were counted directly under a fluorescent microscope or from photomicrographs of sections containing the medial agranular and anterior cingulate cortex. Percentages were calculated from the number of dual-labeled cells (Venus plus GABA) divided by the total population of single-labeled cells (Venus or GABA).

Slice Preparation and Whole-Cell Recording

Oblique horizontal sections with 300 μm thickness were cut along the line of rhinal fissure from rat frontal cortex (19–23 days postnatal), immersed in a buffered solution (NaCl, 124.0; KCl, 3.0; $CaCl_2$, 2.4; $MgCl_2$, 1.2; $NaHCO_3$, 26.0; NaH_2PO_4, 1.0; glucose, 10.0; in mM) aerated with a mixture of 95% O_2 and 5% CO_2. Cells in the frontal cortex (medial agranular and anterior cingulate cortex) were visualized using a 40× water immersion objective, and recorded in whole-cell current-clamp mode at 32 °C. The electrode solution for the current-clamp recording consisted of potassium gluconate 130, NaCl 1.8 $MgCl_2$ 1.8, adenosine triphosphate 2.8, guanosine triphosphate 0.3, 4-(2-hydroxyethyl)-1-piperazineethanesulfonic acid 10, and biocytin 20 mM. The pH of the solution was adjusted to 7.3 with KOH and the osmolarity was adjusted to 290 mOsm. The recorded Venus-expressing cells were observed by direct visual inspection, combined with Nomarski optics, in fluorescence microscope (BX50WI, Olympus, Tokyo, Japan). Current-clamp recordings were made in a fast current-clamp mode of EPC9/dual (HEKA, Lambrecht/Pfalz, Germany; WaveMetrics, Lake Oswego, OR). Electrophysiological data were analyzed by IGOR Pro (WaveMtrics). Cellular input resistance was determined from the membrane response to small hyperpolarizing current injections (<100 pA, 0.5 s duration). Spike widths at half amplitude were measured from spikes elicited by brief (10 ms) depolarizing current injections, whereas the presence of low-threshold (LTS) or burst-spiking behavior was assessed using just-threshold current injection from a starting potential of −75 to −85 mV.

Physiological Identification of Nonpyramidal Cells

Cortical nonpyramidal cells are physiologically heterogeneous and have been classified according to their patterns of action potential generation in response to depolarizing current pulses, and have been divided into 3 broad subclasses: fast-spiking (FS) cells, late-spiking (LS) cells, and non-FS neurons (Kawaguchi and Kubota 1997; Kawaguchi and Kondo 2002; Karube et al. 2004). FS cells are characterized by nonadapting, repetitive spike discharges at a threshold frequency of 40–150 Hz. At just-threshold current levels, FS cell discharges consist of either single spikes at the beginning of the current pulse or irregular bursts of high frequency spike generation with constant spike intervals interspersed. LS cells are characterized by a slow ramp depolarization and delayed action potential firing following just-threshold current injections. Non-FS cells are more heterogeneous in their electrophysiological characteristics than are FS and LS neurons. Some common non-FS cells are LTS neurons (also known as burst-spiking nonpyramidal [BSNP] neurons), regular-spiking non-pyramidal (RSNP) cells, and irregularly spiking neurons, which we have classified here as either BSNP or RSNP cells according to the presence of an initial LTS-like hump (Kawaguchi and Kubota 1996).

Immunohistochemical and Morphological Analysis of Recorded Cells

Tissue slices containing biocytin-loaded cells were fixed by immersion in 4% paraformaldehyde and 0.2% picric acid overnight, followed by a freeze-thawing procedure in sucrose-containing PB using liquid nitrogen twice. Slices were resectioned to a thickness of 50 μm, and were processed for fluorescence immunohistochemistry. Slices were incubated with a primary antibody in TBS containing 2% BSA, 10% NGS, and 0.1% TX. The primary antibody was antiparvalbumin (mouse; 1:4000), antisomatostatin (rat; 1:250), or anti-α-actinin-2 (mouse monoclonal; 1:100,000). After washing in TBS, they were incubated in a Alexa 594-conjugated secondary antibody in TBS containing BSA, NGS, and 0.1% TX for 2 h, followed by incubation with Alexa 350 streptavidin (1:4000; S-11249, Molecular Probes) in TBS for 40 min. After examination for fluorescence, the slices were incubated with ABC complex in TBS containing 0.04% TX, and reacted with DAB and H_2O_2 in TB. They were then postfixed in 1% OsO_4 in PB for 20 min, dehydrated, and flat-embedded on glass slides in Epon. Somata, axons, and dendrites were reconstructed 3-dimensionally using the Neurolucida system (MicroBrightField, Williston, VT). The proportion of boutons in apposition with other somata was calculated from more than 200 randomly sampled boutons.

Data are given as mean ± standard deviation (SD). Analysis of variance (ANOVA) was used for confirmation of significant differences among subtypes in individual parameters, followed by post hoc Tukey test for the group comparison.

Results

Generation of BAC Transgenic Rats

A BAC construct harboring a modified VGAT allele (Fig. 1*A*) was made as described in the Methods. The modified BAC construct included 102 kb upstream of the VGAT gene, and 25 kb downstream. As the VGAT gene itself is only 5 kb (Ebihara et al. 2003), all of the VGAT gene's regulatory regions are likely included within the BAC. Although eGFP is a well-known in vivo marker, we used Venus, a derivative of yellow fluorescent protein (YFP), in place of eGFP because of its enhanced fluorescence (~20-fold brighter than eGFP; Nagai et al. 2002).

Two founder rat lines carrying the VGAT-Venus transgenes were identified by PCR analysis and maintained on a Wistar background. Both lines (lines A and B) transmitted the transgene to their progeny, and lines A and B were named VGAT-Venus-A and VGAT-Venus-B, respectively. Both lines of transgenic rats were characterized for transgene expression, and Venus expression could be observed at postnatal days 1–2 through the skin and skull by fluorescence microscopy.

Both lines of VGAT-Venus transgenic rats exhibit normal growth and reproductive behavior. To confirm the normal production of GABA, we compared the GABA content to total

protein in the cerebrum and cerebellum in VGAT-Venus transgenic rats and their Venus-negative littermates (taking the means of wild-type rats as 100%). VGAT-Venus-A expressing brains had a GABA content ($n = 7$; 103.7 ± 11.3% in cerebrum; 101.3 ± 14.4 in cerebellum) similar to that found in wild-type littermates ($n = 7$; 100.0 ± 8.4% in cerebrum and 100.0 ± 11.4 in cerebellum). VGAT-Venus-B brains also contained similar GABA content ($n = 6$; 103.1 ± 10.1% in cerebrum; 96.7 ± 12.2% in cerebellum) to that of their wild-type littermates ($n = 6$; 100.0 ± 10.3% in cerebrum and 100.0 ± 15.9 in cerebellum). In addition to having normal GABA, the brain structures of both lines showed no abnormalities at the macroscopic level (Fig. 2), and in sections from fixed brains we observed many fluorescent cells. Fluorescence was evident not only in somata, but also in dendrites and axonal boutons (Fig. 1*B–D*).

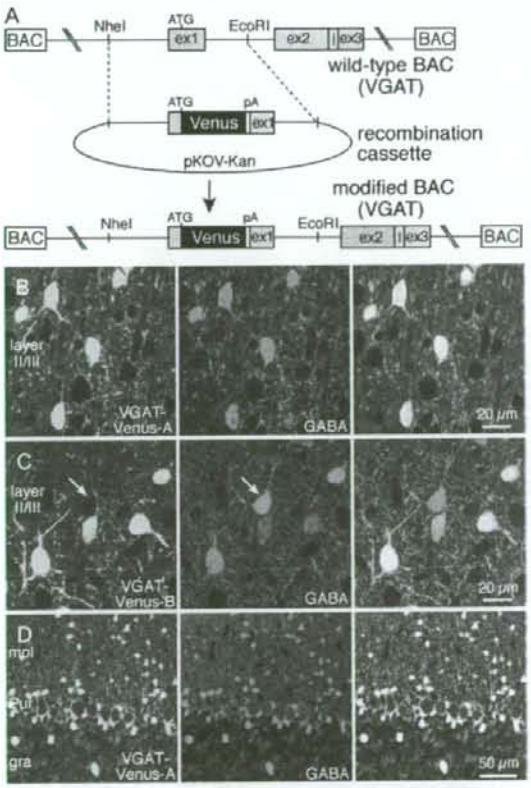

Figure 1. Generation of BAC transgenic rats with Venus fluorescence in VGAT (vesicular GABA transporter)-expressing neurons. (*A*) Schematic representation of the structure of BAC #160L22 containing the VGAT gene (top; wild-type BAC), the recombination cassette (middle), and the modified BAC (bottom). Venus cDNA followed by a poly-A signal was placed into exon 1 of the VGAT gene in frame with the translational initiation codon, ATG. (*B–D*) Colocalization of Venus fluorescence and GABA immunoreactivity in the cerebral and cerebellar cortex of VGAT-Venus transgenic rats. (*B*) Venus-positive cells (left) almost completely overlapped with the GABA-positive population (middle) in layer II/III of the frontal cortex in the "A" line of VGAT-Venus (VGAT-Venus-A) rats. The 2 fluorescence images are merged at the right. (*C*) Venus-positive cells (left) mostly overlapped with the GABA-positive population (middle) in the "B" line of VGAT-Venus (VGAT-Venus-B) rats. However, a few cells were positive for GABA but not for Venus (arrow). The 2 fluorescence images are merged at the right. (*D*) Venus-positive cells (left) in the molecular and granular layer of the cerebellar cortex almost completely overlapped with the GABA-positive population (middle) in VGAT-Venus-A rats, whereas Purkinje cells displayed little Venus fluorescence. GABA immunofluorescence was also weak in Purkinje somata. Abbreviations: mol, molecular layer; Pur, Purkinje cell layer; gra, granule cell layer.

Venus Expression Patterns

To confirm whether Venus-expressing cells are also GABAergic in the neocortex, Venus and GABA immunofluorescence were compared in the frontal cortex (Fig. 1*B–D*). About 98% of Venus-positive cells in line A- and ~95% of Venus-positive cells in line B-animals were also positive for GABA (Table 1). Conversely, in line A, almost all GABA cells displayed Venus fluorescence (Fig. 1*B*), indicating GABA and Venus cells comprise almost completely overlapping populations of neurons in the frontal cortex (Table 1). On the other hand, in the B line, GABA-positive cells in deeper cortical layers were mostly positive for Venus, but some GABAergic cells in the superficial layers, especially layer I, did not express Venus (Fig. 1*C*). This indicates that Venus-positive cells in the frontal cortex of VGAT-Venus-B rats are GABAergic, but that not all GABAergic cells express Venus, especially in layer I (Table 1).

Colocalization of Venus and GABA immunofluorescence was also investigated in the cerebellar cortex of VGAT-Venus-A animals. In the granule cell layer, a few large, putative Golgi cells, had Venus fluorescence that completely overlapped with GABA immunofluorescence (38 cells positive for both Venus and GABA; Fig. 1*D*). Venus cells in the molecular layer also greatly overlapped with GABA-positive cells (484 Venus cells among 492 GABA cells, 98.4%). In contrast, GABAergic Purkinje cells showed only weak Venus fluorescence. GABA immunofluorescence was also weak at their somata (Fig. 1*D*). These data indicate that GABAergic interneurons and Venus cells show a high degree of overlap in the cerebral and cerebellar cortices of transgenic rats, especially in the A line, which had an almost complete overlap of GABA-positive and Venus-positive neurons.

We next compared the Venus and GABA expression patterns in the 2 VGAT-Venus lines, and in wild-type rats, in various brain regions using specific antibodies and DAB staining (Figs 2 and 3).

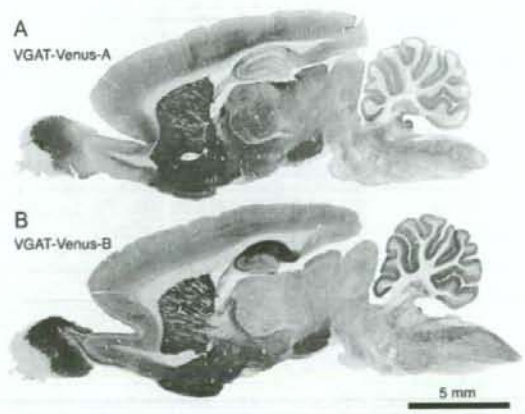

Figure 2. Distribution patterns of Venus in VGAT-Venus rats. Venus was visualized in parasagittal brain slices using the antibody and peroxidase DAB reaction. (*A*) Venus expression in a VGAT-Venus-A rat. (*B*) Venus expression in a VGAT-Venus-B rat. In the forebrain, Venus distribution was similar to that of GABA, except in the hippocampal CA1 region in VGAT-Venus-B rats and thalamus in VGAT-Venus-A rats.

Neocortex

As was found in the frontal cortex, described above, other cortical regions in both animal lines had Venus-positive cells in all layers. In A line animals, Venus cells in layers I–V were positive for GABA. In addition to the expected GABA-positive neurons, layer VI of nonfrontal cortical regions also had some neurons that were faintly labeled with Venus but negative for GABA. In the B line, Venus-expressing cells in layers I–VI were positive for GABA. In addition, in B line animals, a few pyramidal cells in the ventral cortex showed weak Venus fluorescence but were negative for GABA.

Table 1

Relation of Venus fluorescent cells and GABA immunopositive cells in frontal cortex

	VGAT-Venus-A		VGAT-Venus-B	
Layer	Venus/GABA	GABA/Venus	Venus/GABA	GABA/Venus
I	98.6 ± 1.4 (148)	100 ± 0.0 (146)	55.3 ± 4.2 (153)	99.4 ± 1.1 (88)
II/III	97.3 ± 3.6 (1387)	98.6 ± 2.3 (1364)	93.7 ± 0.3 (1551)	98.5 ± 0.7 (1477)
V	97.7 ± 2.5 (1075)	98.5 ± 2.0 (1064)	98.9 ± 0.3 (998)	98.1 ± 2.4 (1011)
VI	98.0 ± 2.1 (1172)	98.7 ± 1.5 (1163)	98.9 ± 0.4 (1342)	99.1 ± 0.8 (1347)
Total	97.6 ± 2.8 (3782)	98.7 ± 1.8 (3737)	95.3 ± 0.5 (4044)	98.7 ± 1.1 (3923)

Note: Data are percentages and mean ± SD of 3 animals. (), total numbers of GABA or Venus cells of 3 VGAT-Venus-A or -B rats.

Hippocampus

In VGAT-Venus-A rats, nonpyramidal cells were labeled with Venus, but no Venus was detected in pyramidal cells in the CA1–3 regions, or in granule cells in the dentate gyrus (Fig. 3*A*), indicating that Venus cells overlap with GABAergic neurons. In VGAT-Venus-B rats, nonpyramidal cells were selectively labeled with Venus in CA2, CA3, and dentate gyrus, but in CA1 both pyramidal and nonpyramidal cells showed fluorescence at their somata and dendrites (Fig. 3*B*).

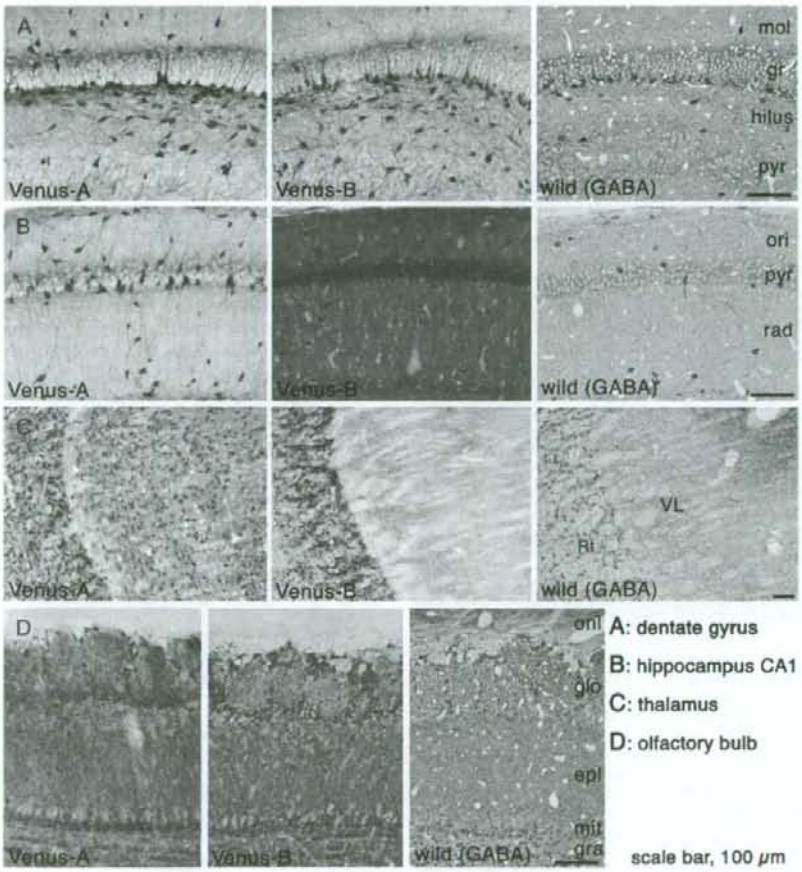

Figure 3. Comparative distribution of Venus-positive cells in 2 lines of VGAT-Venus rats and GABA-positive cells in wild-type rats. Venus expression was more clearly seen in somata than was GABA immunoreactivity. (*A*) Dentate gyrus and CA3 region of the hippocampus: nonpyramidal cells, but not granule or pyramidal cells, expressed Venus in both animal lines. (*B*) CA1 regions of the hippocampus: only nonpyramidal cells expressed Venus in the VGAT-Venus-A rat, but pyramidal cells also expressed Venus in the VGAT-Venus-B rat. (*C*) Thalamus: reticular nucleus cells expressed Venus in both lines of VGAT-Venus rats, but Venus was found in other nucleus in the VGAT-Venus-A rats. (*D*) Olfactory bulb: periglomerular and granule cells were stained in both lines. In the external plexiform layer, dendrites of granule cells were stained. Abbreviations: mol, stratum moleculare; gr, stratum granulare; pyr, stratum pyramidale; ori, stratum oriens; rad, stratum radiatum; Rt, reticular nucleus; VL, ventrolateral nucleus; onl, olfactory nerve layer; glo, glomerular layer; epl, external plexiform layer; mit, mitral cell layer; gra, granular layer.

Thalamus

Venus expression was found in the GABAergic reticular nucleus of both lines (Fig. 3*C*). Further, the lateral geniculate nuclei in both lines contained Venus-positive cells that likely correspond to GABAergic interneurons. In VGAT-Venus-A rats, Venus-positive cells were also found in projection neurons (likely glutamatergic) in other thalamic nuclei such as the ventrolateral, ventroposterior, and laterodorsal nuclei. Thalamic projection cells were not labeled with Venus in VGAT-Venus-B rats.

Olfactory Bulb

Excitatory mitral and tufted cells did not express Venus, whereas granule and periglomerular cells, considered to be GABAergic, were labeled with Venus (Fig. 3*D*). In the granule and inner plexiform layers, a few Venus-positive large cells existed, perhaps corresponding to so-called "short axon cells." The external plexiform layer also had a few large Venus-positive cells that may also belong to the short axon cell group or to other unidentified subtypes. No differences were found in the distribution patterns of Venus-positive cells between the 2 lines.

Basal Ganglia Nuclei

Venus was expressed in GABAergic cells in the basal ganglia of both VGAT-Venus-A and -B animals. In the striatum most cells expressed Venus, indicating labeling of GABAergic projection cells. Qualitatively, most parvalbumin, somatostatin, and calretinin cells were fluorescently labeled in VGAT-Venus-A rats, but large cells positive for choline acetyltransferase were devoid of Venus. Parvalbumin cells showed stronger fluorescence than other types. In both the globus pallidus and entopeduncular nucleus, large multipolar cells were labeled with Venus, corresponding to GABAergic principal cells. The subthalamus showed no Venus fluorescence, whereas many Venus cells were found in zona incerta. In the substantia nigra, the pars reticulata had many Venus cells, corresponding to GABAergic output cells, whereas no Venus cells were localized in the dopaminergic neurons of the pars compacta.

Venus in Cortical GABA Cell Subtypes

To determine whether various GABAergic cell subtypes were labeled with Venus, we investigated colocalization patterns of Venus with the chemical markers for cortical GABAergic cells: parvalbumin, somatostatin, VIP, CCK (Fig. 4*A–D*). Further, we examined the colocalization of Venus and α-actinin-2, an actin-binding protein expressed by some GABAergic neurons in the hippocampus (Ratzliff and Soltesz 2001). In VGAT-Venus-A rats, α-actinin-2–positive cells in all layers also expressed Venus (100% in all layers; Table 2), suggesting that all α-actinin-2–positive cells are GABAergic (Fig. 4*F*). Calretinin is also expressed in GABAergic neurons (Kubota et al. 1994), but we found calretinin immunofluorescence to be variable in intensity. Most cells with strong immunofluorescence also had Venus fluorescence, but some cells with weaker labeling were devoid of Venus in VGAT-Venus-A rats (Fig. 4*E*), suggesting that some non-GABAergic cells may express calretinin (Melchitzky et al. 2005). Therefore, Venus expression was quantitatively analyzed for colocalization with biochemical markers other than calretinin (Table 2). However, we also calculated the proportion of cells expressing all of the above biochemical markers, including calretinin, among the total Venus-positive population (Table 3).

In VGAT-Venus-A rats, cells positive for parvalbumin, somatostatin, VIP, CCK, or α-actinin-2 were almost always positive for Venus (Table 2). This result is consistent with the finding that Venus cells overlap fully with GABAergic cells in the VGAT-Venus-A line. In VGAT-Venus-B rats, the vast majority of parvalbumin and somatostatin cells were also positive for Venus, but a few VIP and CCK cells, and many α-actinin-2 cells were negative for Venus (Table 2). These data suggest that GABAergic cells negative for Venus in VGAT-Venus-B correspond to subpopulations of VIP, CCK, and especially α-actinin-2 cells.

Composition of Cortical GABAergic Population

Because the Venus-positive neuron population overlapped completely with GABA immunoreactivity in VGAT-Venus-A rats, we were able to measure the proportion of each chemical subtype in the total GABAergic (Venus-positive) population in 3 rats. This method, using Venus-expressing tissue, was found to be both easier and more reliable than doing double immunostaining with antibodies to both GABA and a second chemical marker (Fig. 4*A–F*). The mean values obtained from 3 rats are shown in Table 3 and Figure 4*G*. Parvalbumin-positive cells were not found in layer I neurons expressing Venus, but made up 36.4% of Venus-positive cells in layer II/III, 52.7% of cells in layer V, and 38.7% of cells in layer VI. Somatostatin-positive cells were not found in layer I Venus-positive cells, but made up 17.4% of cells in layer II/III, 28.6% of cells in layer V, and 29.0% of cells in layer VI. VIP-positive cells made up 3.3% of layer I Venus-positive cells, 24.0% of cells in layer II/III, 9.6% of cells in layer V, and 8.0% of cells in layer VI. Calretinin cells comprised 35.8% of Venus cells in layer I, 21.0% of cells in layer II/III, 11.1% of cells in layer V, and 11.4% of cells in layer VI. CCK was found in just 0.9% of cells in layer I, 8.9% of cells in layer II/III, 2.9% of cells in layer V, and 3.0% of cells in layer VI. Finally, α-actinin-2–positive cells comprised 66.5% of Venus-positive cells in layer I, 9.8% of cells in layer II/III, 1.5% of cells in layer V, and 6.2% of cells in layer VI.

To estimate the proportion of all GABAergic cells expressing the above 6 chemical markers, their colocalization patterns should be known. Parvalbumin and somatostatin cells were completely independent groups and were also devoid of the other 3 chemical markers (Kubota et al. 1994; Gonchar and Burkhalter 1997; Kubota and Kawaguchi 1997). Coexistence of calretinin and CCK was found in a few cells. Among VIP-positive cells, calretinin was expressed in 33% in layer II/III, 71% in layer V, and 54% in layer VI. Among VIP-positive cells, CCK was expressed in 32% in layer II/III, 21% in layer V, and 19% in layer VI (Kubota and Kawaguchi 1997 and related unpublished observations). Results of the α-actinin-2 colocalization with the other chemical markers in wild-type rats are available in the Appendix below (Fig. 8, Table 5). Parvalbumin-positive and somatostatin-positive cells did not express α-actinin-2, and only a very few VIP-positive and CCK-positive neurons were positive for α-actinin-2. Some α-actinin-2-positive cells showed calretinin immunoreactivity, especially in layer I (14.8%), layer V (18.8%) and layer VI (16.2%). Assuming the colocalization of α-actinin-2 and calretinin in addition to the previously revealed relationships, these 6 chemical markers cover more than 90% of the total GABAergic populations in layers I, II/III, and V, and nearly 90% of cells in VI (Fig. 4*G*).

Functional Characteristics of Venus Cells

To determine whether Venus-expressing cells have differentiated normally into GABAergic cell subtypes, Venus-positive cells

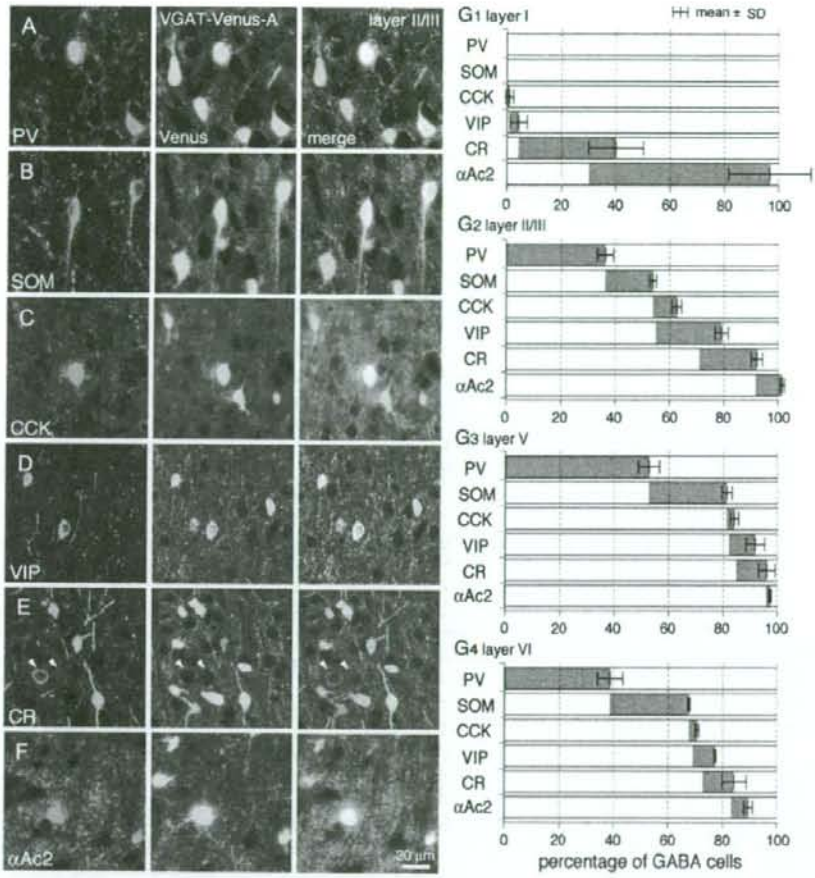

Figure 4. Chemical composition of cortical GABAergic population. (*A–F*) Venus expression in chemically identified cells in layer II/III of VGAT-Venus-A rats. (*A*) Photomicrographs from the same microscopic field, showing the relationship of parvalbumin (PV) and Venus cells. (*B*) Somatostatin (SOM) cells. (*C*) CCK cells. (*D*) VIP cells. (*E*) Calretinin (CR) cells. (*F*) α-Actinin-2 (αAc2) cells. Almost all cells positive for markers other than calretinin expressed Venus. Some calretinin cells (arrows) showed no Venus fluorescence. Calretinin immunofluorescence in these non-Venus labeled neurons was generally weaker than in cells expressing Venus. (*G*) Graph showing the proportion of GABAergic neurons found to express specific chemical markers, including α-actinin-2 (αAc2) cells. The proportion was calculated from 3 VGAT-Venus-A rats. (*G1*) Layer I. (*G2*) Layer II/III. (*G3*), Layer V. (*G4*) Layer VI. Individual bars were displaced to show the overlap in the colocalized portion with another marker. Considering the colocalization patterns of the 6 markers, more than 90% of GABA cells were found to express at least one of the 6 chemical markers in layers I, II/III, and V.

in the cortex were examined for their physiological, morphological, and chemical characteristics (Kawaguchi and Kondo 2002). In layer V of the frontal cortex of VGAT-Venus-A rats, we made whole-cell recordings from FS, RSNP, and BSNP cells. Among 12 recorded FS cells in layer V, 11 cells showed parvalbumin immunoreactivity (Fig. 5*A*), of which 9 cells were identified as basket cells with similar morphology to cells in the wild-type animals (Fig. 5*C2,D*). The remaining 3 FS cells were not morphologically identified because of poor axonal staining. Seven RSNP cells in layer V were immunoreactive for somatostatin, of which 5 cells were Martinotti cells with ascending axonal arbors similar to those found in wild-type rats. Of 8 somatostatin-positive BSNP cells, 6 had morphologies consistent with Martinotti cells (Fig. 5*C1*). Parvalbumin-positive FS cells had more negative resting potentials, smaller input resistances, and shorter spike widths than did somatostatin-positive cells (Table 4), and somatostatin-positive BSNP cells had larger input resistances than RSNP cells (Kawaguchi and Kubota 1996).

To confirm the differentiation of VIP cells, we identified 5 Venus-expressing VIP-positive cells in layer II/III (Fig. 6*A*), among which 2 cells well stained showed the descending axonal arbors morphologically. Physiologically, they included cells with either strong firing adaptation or irregular spiking (Fig. 6*B,C*), and were classified as either RSNP or BSNP. Thus, we found no differences in the physiological, chemical, and morphological characteristics between wild-type and VGAT-Venus rat. These data suggest normal functional differentiation of cortical GABAergic cells in VGAT-Venus rats.

Although most GABAergic cell subtypes can be labeled with calcium-binding proteins and neuropeptides, specific chemical markers have not previously been identified in neocortical LS

neurogliaform cells. In hippocampus, α-actinin-2 is expressed not only in dendrites of pyramidal cells, but also in somata of interneurons (Wyszynski et al. 1998; Ratzliff and Soltesz 2001), including neurogliaform cells (Price et al. 2005). We investigated whether LS cells coincide with the α-actinin-2–positive cell population in frontal cortex. Immunofluorescence for α-actinin-2 was investigated in LS cells whose somata were well stained ($n = 6$ in layer II/III and $n = 2$ in layer V). Five LS cells were positive for α-actinin-2 in layer II/III and both positive in layer V (Fig. 5*B,C3*). LS neurogliaform cells positive for α-actinin-2 had more hyperpolarized resting potentials than somatostatin cells, longer spike widths than parvalbumin FS cells, and lower input resistances than somatostatin BSNP cells (Table 4).

To further reveal the functional differentiation between parvalbumin, somatostatin, and α-actinin-2 cells, we compared their firing characteristics quantitatively. Parvalbumin FS cells required more current to induce spikes than was required in α-actinin-2 LS cells or somatostatin BSNP cells (Fig. 5*E*). When depolarized just above action potential threshold, parvalbumin and α-actinin-2 cells fired spikes at relatively constant intervals, whereas somatostatin cells showed spike-frequency adaptation. Parvalbumin-positive FS, somatostatin-positive RSNP, and α-actinin-2–positive LS cells increased their firing rate linearly with larger amplitude current injections (up to 500 pA) (Fig. 5*F*). The slope of firing frequency verses injected current (duration, 0.5 s) was 270 Hz/nA in parvalbumin FS cells (correlation coefficient [c.c.] = 0.65), 163 Hz/nA in somatostatin RSNP cells (c.c. = 0.92), and 34 Hz/nA in α-actinin-2 LS cells (c.c. = 0.65), indicating significant differences in the output characteristics of these neurons.

Table 2
Colocalization of chemical markers for GABAergic nonpyramidal cells with Venus in frontal cortex of VGAT-Venus rats

Layer	PV	SOM	VIP	CCK	αAc2
VGAT-Venus-A					
I	No cells	No cells	100% (6)	100% (4)	100% (104)
II/III	99.8% (470)	98.6% (142)	98.3% (359)	100% (165)	100% (154)
V	100% (378)	96.2% (132)	98.8% (85)	100% (28)	100% (15)
VI	99.7% (306)	98.1% (211)	97.6% (85)	97.7% (43)	100% (52)
Total	99.8% (1154)	97.7% (485)	98.3% (535)	99.6% (240)	100% (325)
VGAT-Venus-B					
I	No cells	No cells	28.6% (7)	0.0% (1)	47.0% (134)
II/III	99.7% (622)	98.2% (336)	88.5% (226)	88.9% (235)	59.6% (136)
V	99.9% (731)	98.8% (248)	95.0% (60)	82.9% (41)	85.7% (14)
VI	99.7% (751)	98.4% (189)	95.1% (61)	94.8% (58)	74.5% (47)
Total	99.8% (2104)	98.4% (773)	89.5% (354)	89.0% (335)	57.7% (331)

Note: Venus cells/cells positive for a chemical marker. Data are combined from 3 animals in A line, 2 animals in B line. ( ), number of cells positive for individual chemical markers (denominator). PV, parvalbumin; SOM, somatostatin; αAc2, α-actinin-2.

To assess further the differentiation of Venus-expressing GABAergic cells, we examined the dendritic morphology and synaptic innervation patterns of neurons exhibiting physiological and chemical correlations. The number of dendrites issuing from the soma (primary dendrites) was 6.2 ± 1.6 ($n = 9$; range, 4–9) in parvalbumin-positive FS basket cells, 6.0 ± 1.8 ($n = 6$; range, 4–9) in α-actinin-2–positive LS neurogliaform cells, and 3.2 ± 0.8 ($n = 11$; range, 2–4) in somatostatin-positive Martinotti cells (which were significantly fewer than in the above FS and LS cells, $P < 0.01$).

In a previous study, we used electron microscopy to confirm that about 80% of visually identified (via light microscopy) nonpyramidal neuron axonal boutons apposed to somata make synaptic junctions onto them (Karube et al. 2004). Here we also used Nomarski optics to identify appositions of intracellularly stained axonal boutons onto unstained postsynaptic somata (Fig. 5*D*). For 3 nonpyramidal cell subtypes (FS, Martinotti, and LS cells), we measured the number of stained boutons apposed to other somata as a proportion of the total number of boutons observed. Boutons arising from parvalbumin-positive FS basket cells and somatostatin-positive Martinotti cells targeted somata in 22.3 ± 4.3% and 2.5 ± 1.9%, respectively ($P < 0.01$; Fig. 5*G*). The proportion of somatic apposition in boutons from α-actinin-2–positive LS neurogliaform cells was 14.3 ± 6.4% (larger than the above somatostatin Martinotti cells, $P < 0.01$; smaller than the above parvalbumin FS cells, $P < 0.05$) (Fig. 5*G*), and in addition showed more variability within its group than other subtypes. A comparison of these results with those of wild-type rats is available in the Appendix (Fig. 9), and confirms that the proportion of soma-targeting boutons is similar in wild-type and VGAT-Venus rats. These observations suggest that α-actinin-2–positive LS neurogliaform cells are unique compared with the other cell subtypes in the aspects of physiology, dendritic elongation and innervation targets.

FS Basket Cells Heterogeneous in their Somatic Size and Dendritic Territory

When recording in wild-type rats, we identified cortical GABAergic nonpyramidal cells on the basis of their somatic shape and size. Layer V contains a few large nonpyramidal cells with somatic sizes comparable with pyramidal cells, or having pyramid-shaped somata (Marin-Padilla 1969; Jones 1975; DeFelipe et al. 1986). This has made discriminating these large nonpyramidal cells from the abundant population of pyramidal cells difficult. Although their number is small, large interneurons may play an important role in cortical function (Hensch 2005). Recording from slices of VGAT-Venus rat, we found large FS cells that were of similar size or shape to pyramidal cells (Fig. 7*A*). The maximum cross-sectional areas of layer V FS cells recorded from Venus rats were 220 ± 67 μm^2 (maximum = 356

Table 3
Mean percentages of cells positive for individual chemical markers among Venus cells of frontal cortex in 3 VGAT-Venus-A rats

Layer	PV	SOM	VIP	CR	CCK	αAc2
I	No cells (118)	No cells (63)	3.3 ± 3.2 (121)	35.8 ± 10.1 (78)	0.9 ± 1.5 (214)	66.5 ± 15.2 (173)
II/III	36.4 ± 2.9 (1284)	17.4 ± 1.4 (828)	24.0 ± 2.5 (1473)	21.0 ± 2.1 (1236)	8.9 ± 1.8 (1972)	9.8 ± 0.8 (1579)
V	52.7 ± 3.9 (726)	28.6 ± 1.9 (450)	9.6 ± 3.5 (857)	11.1 ± 3.1 (576)	2.9 ± 1.5 (1096)	1.5 ± 0.4 (1003)
VI	38.7 ± 4.6 (801)	29.0 ± 0.4 (713)	8.0 ± 0.3 (1048)	11.4 ± 4.4 (907)	3.0 ± 0.7 (1437)	6.2 ± 1.6 (847)
Total	39.3 ± 1.4 (2929)	23.4 ± 1.3 (2054)	15.0 ± 0.7 (3499)	16.1 ± 2.7 (2797)	5.5 ± 1.1 (4719)	8.9 ± 1.2 (3602)

Note: Mean ± SD of 3 VGAT-Venus-A rats. PV, parvalbumin; SOM, somatostatin; CR, calretinin; αAc2, α-actinin-2. (), total numbers of Venus cells of 3 VGAT-Venus-A rats.